CTH-NT-256

Thesis for the degree of
Doctor of Philosophy

Neutronics in reactors with propagating perturbations

Anders Jonsson

Nuclear Engineering
Department of Applied Physics
Chalmers University of Technology
S-412 96 Göteborg, Sweden 2012

Neutronics in reactors with propagating perturbations
ANDERS JONSSON
ISBN 978-91-7385-703-1

Doktorsavhandling vid Chalmers tekniska högskola
Ny serie nr 3384
ISSN 0346-718X

Nuclear Engineering
Department of Applied Physics
Chalmers University of Technology
S-412 96 Göteborg
Sweden
Telephone +46 (0)31 772 1000
Fax +46 (0)31 772 3872

Cover: Simplified schematic of a Molten Salt Reactor. Adapted from Fig. 3.1.

Chalmers Reproservice
Göteborg, Sweden 2012

Neutronics in reactors with propaging perturbations
ANDERS JONSSON
Nuclear Engineering
Department of Applied Physics
Chalmers University of Technology

ABSTRACT
This thesis contains several studies of the properties of neutron noise, primarily in Molten Salt Reactors and other reactors with propagating perturbations. Both one- and two-group diffusion theory are employed to investigate the differences that arise from the movement of the fuel. Data corresponding to a thorium-fuelled thermal reactor is used to investigate the properties of a more realistic possible realisation of an MSR system, as well as data corresponding to more traditional systems for contrast. Furthermore, the properties of the neutron noise from a vibrating absorber or fuel rod in a traditional reactor is investigated in a two-group, multi-region system.

For the MSR, the Green's functions and the dynamic adjoint functions are investigated in the general case of arbitrary fuel recirculation velocity and in the limiting case of infinite fuel velocity which permits simplified solutions both in the static and dynamic case. It is found that the amplitude of the induced noise is generally higher and the domain of the point kinetic behaviour valid up to higher frequencies than in a corresponding traditional system. This is due to the differing behaviour of the delayed neutron precursors as compared to the traditional case.

The MSR equations are not self-adjoint and the adjoint equations and adjoint functions have to be constructed, which is also done here. Finally, the space-dependent neutron noise, induced by propagating perturbations of the absorption cross section is calculated. A number of interesting properties that are relevant to full size MSRs are found and interpreted. The results are consistent with those in traditional systems but the domains of various behaviour regimes (point kinetic, space dependent etc.) are shifted to higher frequencies or system sizes.

Keywords: neutron noise, Green's function, Molten Salt Reactors, one-group theory, two-group theory, propagating perturbations

SAMMANFATTNING

Denna avhandling omfattar flera studier av egenskaperna hos neutronbrus, huvudsakligen för saltsmältereaktorer och andra system med spridande störningar. De skillnader som uppkommer från bränslets transport undersöks med både en- och tvågruppsteori. Parametrar som motsvarar ett termiskt system med toriumbränsle används för att undersöka egenskaperna hos en realistiskt saltsmältereaktor, liksom parametrar motsvarande mer traditionella system för jämförelse. Vidare undersöks neutronbruset från vibrerande styr- och bränslestavar i en traditionell reaktor i en tvågruppsmodell med flera regioner.

För saltsmältereaktorn undersöks Greensfunktionen och det hermiteska konjugatet både med godtycklig recirkulationstid och med oändlig bränslehastighet. Det senare förenklar lösningarna både i det statiska och det dynamiska fallet. Det visar sig att det inducerade bruset har större magnitud och att giltighetsområdet för punktkinetiskt beteende sträcker sig till högre frekvenser än i motsvarande traditionella system. Detta beror på skillnader i fördelningen av fördröjda neutronföregångare från bränslets rörelse.

Ekvationerna för saltsmältereaktorer är inte självkonjugerade och de konjugerade ekvtionerna och funktionerna måste konstrueras, vilket också görs. Slutligen beräknas rumsberoendet hos neutronbrus från en spridande störning av absorbtionstvärsnittet. Flera intressanta egenskaper hos fullskaliga saltsmältereaktorer har hittats och tolkas. Dessa motsvarar egenskaper hos tradtionella system, men giltighetområdena för dem sträcker sig över högre frekvenser eller systemstorlekar.

Appended publications

This thesis is an introduction to and a summary of the work published in the following papers, referred to by Roman numerals in the text:

Paper I

I. Pázsit and A. Jonsson, "Reactor Kinetics, Dynamic Response, and Neutron Noise in Molten Salt Reactors"
Nuclear Science and Engineering, **167**, 61–76, 2011.

Paper II

A. Jonsson and I. Pázsit, "Two-group theory of neutron noise in Molten Salt Reactors"
Annals of Nuclear Energy, **38**, 6,1238–1251, 2011.

Paper III

I. Pázsit and A. Jonsson, "Kinetic Aspects of Neutron Noise in Molten Salt Reactors"
Invited paper in the session "Advances in Nuclear Reactor Kinetics",
ANS Annual Meeting, Hollywood, Florida, 26-30 June 2011.
Transactions of the American Nuclear Society, **104**, 850, 2011

Paper IV

I. Pázsit, A. Jonsson and L. Pál, "Analytical solutions of the molten salt reactor equations"
Submitted to Annals of Nuclear Energy, 2012.

Paper V

A. Jonsson, H.N. Tran, V. Dykin and I. Pázsit, "Analytical investigation of the properties of the neutron noise induced by vibrating absorber and fuel rods"
Submitted to Kerntechnik, 2012.

Paper VI

V. Dykin, A. Jonsson and I. Pázsit, "Qualitative and quantitative investigation of the propagation noise in various reactor systems"
Submitted to Progress in Nuclear Energy, 2012.

Publications not included in this thesis

Paper I

I. Pázsit, G. Wihlstrand, T. Tambouratzis, A. Jonsson and B. Dahl, "Research and Development Program in Reactor Diagnostics and Monitoring with Neutron Noise Methods",
Stages 14–15, SSM Report 2009:38, Chalmers University of technology, Göteborg, Sweden, December, 2009.

Paper II

I. Pázsit and A. Jonsson, "Reactor Kinetics, Dynamic Response, and Neutron Noise in Molten Salt Reactors"
Proc. of the International Conference of the Physics of Reactors: Advances in Reactor Physics to Power the Nuclear Renaissance (PHYSOR 2010), Pittsburgh, USA, May 9–14, 2010.

Paper III

I. Pázsit, V. Dykin and A. Jonsson, "Final Report: Research and Development Program in Reactor Diagnostics and Monitoring with Neutron Noise Methods",
Stage 16, SSM Report 2010:22, Chalmers University of technology, Göteborg, Sweden, September, 2010.

Paper IV

I. Pázsit and A. Jonsson, "Kinetic Behaviour and Neutron Noise in Molten Salt Reactors"
Proceedings of of GLOBAL 2011, Makuhari, Japan, Dec. 11-16, 2011. Paper No. 392290

Paper V

I. Pázsit, H. N. Tran, V. Dykin and A. Jonsson, "Research and Development Program in Reactor Diagnostics and Monitoring with Neutron Noise Methods",
Stage 17. SSM Report 2011:29, Chalmers University of technology, Göteborg, Sweden, September, 2011.

Paper VI

I. Pázsit, H. N. Tran, V. Dykin and A. Jonsson, "Research and Development Program in Reactor Diagnostics and Monitoring with Neutron Noise Methods",
Stage 18. SSM Report, Chalmers University of technology, Göteborg, Sweden, September, 2012

Contents

1 Introduction **1**

2 Molten Salt Reactors: history and present **3**
2.1 A brief history of Molten Salt Reactors 3
2.1.1 The Molten Salt Reactor Experiment 4
2.2 Recent interest in MSRs 7
2.2.1 Research projects 7

3 Molten Salt Reactors: overview **9**
3.1 Properties of an MSR 9
3.2 MSR neutronics 11
3.3 Thorium fuel 12

4 MSR neutronics in one-group theory **15**
4.1 Basic equations 15
4.1.1 General, analytic solution 17
4.1.2 Boundary conditions 19
4.2 The adjoint 20
4.3 Limiting cases 21
4.4 Time dependent equations 23
4.4.1 Finite velocity 31
4.5 Noise induced by propagating perturbations 34

5 MSR neutronics in two-group theory **39**
5.1 Investigated systems 39
5.2 Comparison with traditional reactors 40
5.3 Basic equations for MSRs 43
5.4 Infinite fuel velocity 44
5.4.1 Dynamic behaviour 47
5.4.2 Propagating perturbation 50
5.5 Finite velocity 57
5.5.1 Static flux 57
5.5.2 Adjoint Green's functions 58

6 Multi-region theory **63**
6.1 Equations 63
6.2 Absorption vibration 64
6.3 Fuel vibration 65

7 Concluding remarks **69**

Acknowledgements **71**

References **74**

CHAPTER 1

INTRODUCTION

Den här skall man vrida på för att lära sig allt om radioaktivitet.
—Tove Jansson, *Mumintrollet och marsinnevånarna*

During the last few years, due to the increasing demands of electricity and the increasing awareness of the problem of global warming, there has been a renewed interest in nuclear power. Nuclear power can not only prevent emissions from fossil fuel plants (including greenhouse gases) but also offers a way of diversifying the energy sources and lessening the reliance on a small set of nations blessed with oil reserves.

Furthermore, Fukushima has underlined the need for new nuclear reactors to be inherently safe, so that a total loss of all backup and external power does not put the reactor in an unsafe state.

The renewed interest is thus not limited to plans for building new reactors using existing technology, but also extends to new designs which promise to be more than just refinements of what exists today, offering not only increased safety, but also better sustainability through breeding, lessened output of nuclear waste or even burning of existing spent fuel. These types of reactors are often referred to as "Generation IV" (for comparison, Generation I was the very first reactors, most of the reactors in use today are Generation II, and the reactors now under construction belong to Generations III and III+).

Six such innovative designs have been selected by the Generation IV International Forum (GIF) as promising candidates for Generation IV reactors: the Gas cooled Fast Reactor (GFR), the Sodium cooled Fast Reactor (SFR), the Lead cooled Fast Reactor (LFR), the Very High Temperature Reactor (VHTR), the SuperCritical Water cooled Reactor (SCWR) and the Molten Salt Reactor (MSR). Of these, the Molten Salt Reactor is the most different from traditional reactors: it operates using a liquid fuel that also acts as coolant[a], which gives rise to differences in not only the thermohydraulic but

[a]There are some designs with liquid salt acting only as coolant as well, which are also sometimes referred to as MSRs, but those have more in common with traditional systems or other Generation IV designs and will not be covered here.

also the basic neutronic properties. Another point of interest is the possible use of the MSR with a thorium fuel cycle, which would greatly increase the potential availability of nuclear fuel.

There have been several studies of the MSR using numerical methods, but these have been mostly focused on either the benchmarking of codes or the studies of transients, and the basic neutronic properties of the MSR have not been studied extensively.

This study presents analytical solutions to the diffusion equations for MSRs, as well as studies of the neutron noise. In addition, to better understand the neutron noise of MSRs, the noise of traditional reactors with perturbations resembling those present in MSRs have also been studied.

Chapters 2 and 3 serve as a background to the MSR reactor, and the use of thorium fuel: Chapter 2 covers the history of the MSR, and Chapter 3 outlines its properties and the advantages and disadvantages when compared to other designs.

Chapter 4 covers one-group theory for the MSR: the diffusion equation is solved exactly, both for the static flux and the Green's function, and the noise from a propagating perturbation is calculated.

Chapter 5 covers two-group theory: similar calculations are made as in the Chapter on one-group theory. Furthermore, traditional systems with propagating perturbations are also examined for comparison.

Chapter 6 covers two-group theory with several regions for traditional reactors. In particular, the fast noise is examined and is shown to be useful for noise analysis.

CHAPTER 2

MOLTEN SALT REACTORS: HISTORY AND PRESENT

Put the switch in the wall
Nuclear power to us all
—S.P.O.C.K. "Electric"

This chapter gives a brief overview of the history of the Molten Salt Reactor concept, from the beginning in the Aircraft Nuclear Propulsion Program, over the Molten Salt Reactor Experiment at Oak Ridge National Laboratory, to the present situation.

2.1 A brief history of Molten Salt Reactors

The Molten Salt Reactor was originally conceived by Ed Bettis and Ray Briant at the Oak Ridge National Laboratory (ORNL) as part of the Nuclear Energy Propulsion of Aircraft (NEPA) program – an attempt by the US Air Force to get nuclear aircraft as a sort of counterpart to nuclear submarines: air planes capable of staying airborne for days without refuelling [1]. The aim was to have the reactor operate at high temperature and cool it with air which would then be used in a jet engine. The MSR design was chosen because the salt would remain stable both under high temperature and high radiation, and because it had a high power density [2]. To reduce the radiation exposure of the crew, one of the ideas was to use two aircrafts, and let the one with the reactor tug the one with crew and nuclear armament. In total, over a billion dollars were spent on developing nuclear-powered air planes [3]. The MSR was also considered for powering equipment in spacecraft [2].

One of the more important parts of the development program was the search for a material to construct the reactor from. What was found was Hastelloy N (then called INOR-8), a nickel-molybdenum-iron-chromium alloy [4].

The development program ran from 1950 to 1958[a]. As part of it, the Air Craft Reactor Experiment (ARE), a small BeO-moderated experimental reactor, ran for 9 days in 1954, with steady state temperature at 860° C, and maximum temperature at 882° C, and a maximum output of 2500 kW thermal power [5]. However, Alvin Weinberg, research director of the ORNL at the time, described the experiment as "nerve racking", with even tiny leaks – and there were many – leading to radiation escaping and alarms setting off. Four hours after final shutdown, the last leak occurred, and radiation levels in the control room reached 2000 times the background [4].

The Air Force was nevertheless pleased with the results and got its two largest engine suppliers into the project. A second reactor was devised and some parts even delivered, but the NEPA project was cancelled in 1960 and this second reactor was left unfinished [4]. The program as a whole did not manage to build any nuclear-powered aircraft, though one plane, a modified B-36, flew several times between 1955 and 1957 with an operational reactor in the bomb bay to test the effect of a running reactor on the aircraft systems [2].

The program was made largely obsolete due to the development of ballistic missiles, midair refuelling, and longer range traditional bombers, which made the radiation hazards to the crew a price too high to pay. The program was cancelled in 1961, but the idea was briefly considered again in the 1970s [2].

At the same time Weinberg tested another reactor at ORNL, an aqueous homogeneous reactor, with uranium dissolved in water but otherwise operating according to similar principles as an MSR. It reached full power in early 1953, and was, according to Weinberg, the second reactor to generate electricity and the first reactor to feed electrical power into a commercial grid (that of Consolidated Edison) [4]. Later the same year, another reactor apparently based on the same design, went critical at North Carolina State College, and was the first civilian research reactor to do so. It was so early that the AEC had not yet begun issuing licenses, and operations instead begun under a direct order. In October 1955, when the license was actually issued, the reactor had been shut down for several months due to corrosion issues, and it never started again [6]. A second, much larger (5000 kW thermal) test reactor at Oak Ridge was started in early 1958, but had problems with the zirconium tanks melting, and was finally shut down in 1961 [4].

2.1.1 The Molten Salt Reactor Experiment

While the plans for a nuclear aircraft were abandoned, the results on MSRs were salvaged by the ORNL, where the development was shifted to the goal of making MSRs viable as civilian reactors. The new program was more of a continuation of the old with a shift in emphasis than anything. This development started already in 1956, when interest in the NEPA had begun to decline [1]. From the ARE program, valuable lessons in fuel chemistry and the general

[a]The end date seems unclear; [1] claims that an "active development program" ran to 1956, [5] that the "work was discontinued" in 1958.

Figure 2.1: The building which housed the ARE and MSRE.

handling of the salt were carried over, as well as the Hastelloy N material [5].

At the beginning of 1960, financial support became dependent on the MSR's capabilities as a breeder reactor (in this capacity called MSBR, Molten Salt Breeder Reactor): it would be possible to operate at thermal conditions since the fuel could be purified continuously, which could compensate for the higher effectiveness of a fast plutonium breeder in the U-238 cycle, or make the thermal Th-cycle breeding of U-233 more efficient [4, 7].

To demonstrate the capability of the MSBR, the Molten Salt Reactor Experiment reactor was built at ORNL. At the time, due to limited knowledge of processing chemistry, the designs of MSBRs included two loops: one for fissile material and one for fertile (this setup does allow for more effective breeding and easier chemistry, but is at the same time more technically complicated). The MSRE was built with only the fissile loop, and designed to operate at near thermal conditions, using graphite as moderator, and three control rods for temperature control and shutdown. The radioactive isotopes of xenon and krypton that were created as fission products were purged in the pump bowl and led through a charcoal bed. The reactor was originally planned to operate at 10 MW, but due to miscalculations of the heat transfer only operated at 8 MW. Apart from that, it was a success: it went critical in June 1965 and was ready for stable operation in December 1966, operated reliably – it had 80% availability between December 1966 and March 1968 – and maintenance could be done safely and without much delay [1, 5].

Experiments were made on xenon stripping, tritium behaviour, deposition of fission products, and, perhaps most impressive, different fuels. The reactor originally ran on a uranium-thorium mixture; at one point, extra plutonium was added, and later, the uranium inventory was switched so the reactor ran on U-233, and was in fact the first reactor ever to run on this fuel [1].

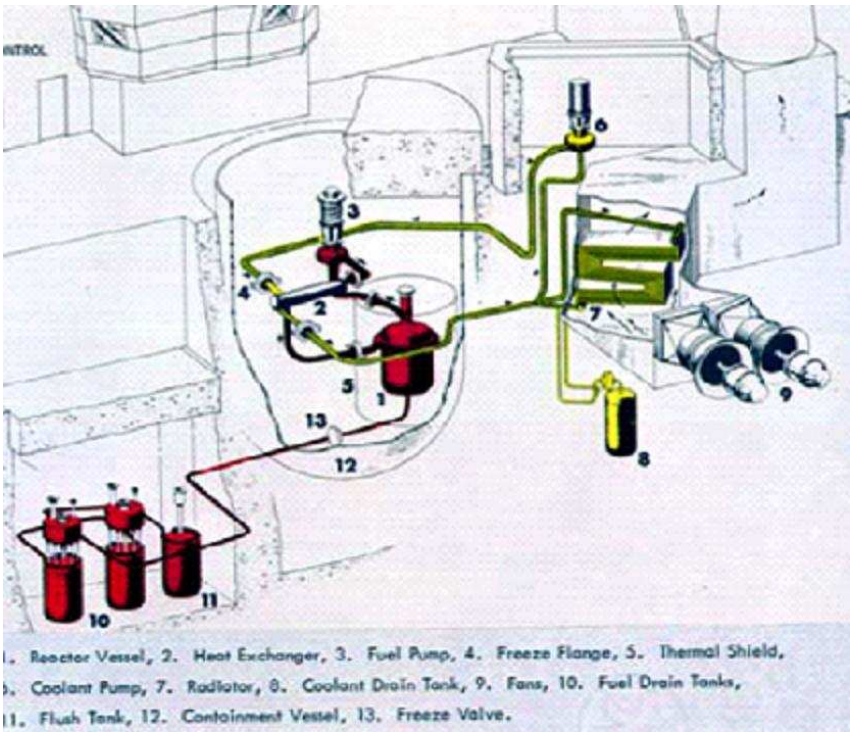

Figure 2.2: Schematic of the MSRE.

The switch to U-233 demonstrated several strong points of the MSR: not only could it be run on several different fuel types without having to be rebuilt, but the handling of the highly radioactive U-233 was done with relative ease, and the removal of the previous inventory of uranium was also very easy: when changing fuel, 218 kg was removed over four days, and it was decontaminated so thoroughly that the gamma radiation dropped by a factor of $4 \cdot 10^9$ [1].

The MSRE operated from 1965 to 1969. The reasons for shutting it down were economical, not technical. It had been reliable, and maintenance was accomplished safely. There had been some problems with the Hastelloy N, as well as the containment of tritium, but these appeared to have been solved, and there seemed to be reason to believe that a larger, actually breeding test reactor would soon be under construction [1]. However, the competition from fast breeding reactors proved too strong: a combination of solutions to the engineering problems being discovered too late in the evaluation process and inertia – funding had already been granted to a program for liquid metal cooled reactors – proved to be too much for the project to survive, and work on the MSR at ORNL was cancelled in 1973 [3, 1]. It was for some reason restarted the year after, but was again cancelled, this time for good, in 1976 [1]. In September 1994, the MSRE was designated an ANS Nuclear Historic Landmark [8].

2.2 Recent interest in MSRs

After the demise of the ORNL program, the interest in MSRs lessened, even if designs have continued to be proposed. These usually focus on the possibility to use either the breeding capabilities of the MSR in a thorium cycle, or to use it as a burner of minor actinides. The interest was renewed when the MSR was selected as one of the Generation IV designs by the Generation IV International Forum (GIF). GIF is a common project of several countries and the European Union (France and the United Kingdom are members both in their own right and through the EU). Their criteria for inclusion of a design in the project are: sustainability (including minimisation of waste), economics, safety and reliability, and proliferation resistance and physical protection [9, 10].

2.2.1 Research projects

In the US, the Accelerator-Driven Neutron Applications (ADNA) corporation of the Los Alamos National Laboratory proposed an MSR design, a thermal, sub-critical accelerator-driven reactor moderated by graphite or heavy water, intended for the destruction of nuclear waste, especially plutonium. It is meant to be a part of a two-tier system, where the first tier burns the waste directly, reducing the amount of material needed to be stored geologically to one fifth of the original. A second, more expensive system for separation and burning of minor actinides is then possible if deemed necessary [11]. Studies have been made on the transmutation capabilities and its dynamical behaviour.

In Europe, several projects have been part of the European Union-financed MOST project (Review on MOlten Salt reactor Technology), aimed at the assessment of available technology to use as a basis for future research programs. The project was needed since even though a large number of experiments had been performed at the ORNL, in the Soviet Union and in Europe in the 60s and 80s, a lot of the experimental data was still not properly analysed. This has been succeeded by other projects that have come to focus on a fast molten salt reactor (MSFR), most recently the EVOL and SUMO projects, for optimisation and feasibility demonstration respectively.

There have also been other projects aimed at producing new knowledge:

- In Russia, work started already in 1976 at the Kurchatov Institute, studying the reactor physics and safety, the structural materials, handling of the salts and the heat transfer [12]. The International Science and Technology Center's Project #1606 was called Experimental Mock-up of Molten Salt Loop of Accelerator-Based Facility for Transmutation of Radioactive Waste and Conversion of Military Plutonium, aimed mainly at investigating the properties of the salt, including the corrosion on a test loop, and calculation on the reactor physics and fuel cycle of a Molten Salt Burner [7].

- The Czech Nuclear Research Institute in Řež is also working on designing a burner called SPHINX (Spent Hot fuel Incineration by Neutron fluX). During the studies, which have lasted over a decade, a sub-critical system was considered, but the program now seems to have settled on a burner without breeding capabilities. The program has also investigated the possible separation technologies.

- In France, a law passed in 1991 calls for research in transmutation technologies as well as long term-storage. As part of the search for a possible transmuter, the AMSTER (Actinides Molten Salt TransmutER) design builds on ORNL's MSBR. Graphite moderated, it aims versatility, to be able to adapt to breeding or transmutation needs, and has been investigated for different fuel types as well as different operating modes [13].

In Japan, there has been a continuous interest in a concept called a FUJI MSR, an attempt at a commercial breeder. The current plans are to start with a 10 MWe test reactor, to be followed later by the full-size reactor delivering 200 MWe.

China has also announced a project for building a thorium-fuelled molten salt reactor.

Apart from these studies with the ultimate aim of building MSRs, there have also been studies made on the properties of MSR systems, using either advanced kinetic approximations [14] or with dedicated ICFM codes [15].

CHAPTER 3

MOLTEN SALT REACTORS: OVERVIEW

Hvarifrån kom torium i en hast?
—August Strindberg, *En blå bok*

This chapter gives an introduction to the concept of the Molten Salt Reactor, explaining why it is of interest. It also takes a look at Thorium as a possible part of a Molten Salt Reactor concept.

3.1 Properties of an MSR

As explained earlier, MSRs run on a liquid fuel, usually taken to be a fluoride salt, mostly consisting of a mixture of different non-fissile materials mixed with fissile and possibly fertile material. This salt circulates, and thus acts both as fuel and coolant. This increases thermal efficiency as the only heat transport needed inside the core is to cool the graphite moderator (the most common choice), which is heated by the radiation.

The reactor core is cylindrical, and in the case of a moderated reactor, contains a cylindrical block of graphite with channels through which the fuel flows; unmoderated reactors typically are considered to consist of one big cylinder without any guidance for the fuel. As the fuel is not pressurised, the ex-core systems are simpler than in traditional reactors, with two interesting extra features: first, in the pump bowl, the fuel is percolated with helium, which causes a release of noble gas fission products, which eliminates poisoning by Xe-135 and ensures that the radioactive gases will not be released to the environment. Second, part of the fuel can be diverted to a chemical plant for online reprocessing. The extent of this reprocessing can vary greatly, from simple refuelling to extraction of undesirable elements and, in the case of a thorium-fuelled reactor, the U-233 precursor Pa-233.

The MSR is quite versatile, and can support several different fuel types, with either a fast or a thermal spectrum. It has good neutron economy, as no

excess fuel is needed to compensate for burn-up – more fissionable material will instead be added to the fuel during operation. This also eliminates the need to add burnable poisons and most of the use of control rods to keep the reactivity stable. The economy is improved further, by the possibility to remove neutron poisons during operation. Since refuelling and processing can be done online, the potential availability will also be high. Also, actinides can be added to the fuel without blending and fabrication.

Because the fuel does not need to be pressurised, the reactor does not need to be contained in a large pressure vessel. The heat transfer properties and temperature of the salt – above 450°C, but usually less than 800°C – lets the reactor operate with high thermal efficiency; one design has a calculated thermal efficiency of 44%.

MSRs are inherently safe, due to a very strong negative temperature coefficient from the expansion of the salt as well as other passive properties or technical solutions, such as meltable barriers which can empty the fuel into containers in case of increased temperature. The chemical stability of the salt increases safety further: the low vapour pressure means that even in the case of a fuel spill, it will be well contained and not lead to a release to the atmosphere. However, the use of graphite as a moderator puts restraints on the design to avoid positive feedback.

Proliferation resistance should, in general, be quite good: there are fewer steps in handling the fuel since there is no fabrication, and since the fuel inventory always will be just slightly above what is needed for criticality, diversion of fuel would quickly stop the reactor from operating. There are some concerns about using the thorium cycle and the production of U-233, but these can be avoided by the right fuel composition or are similar to the problems presented by other types of breeder reactors (more about this in section 3.3).

As can be seen, the MSR fulfils most of the GIF's criteria: the sustainability is good, due to the possibility of running on thorium fuel and the excellent fuel economy, the waste handling is at the very least an improvement over traditional reactors with the possibility of online reprocessing, safety and reliability has been demonstrated to be good, physical protection should be very good due to the low pressure environment and the properties of the salt. Economics are harder to speculate about, but calculations indicate that the cost of electricity from an MSR should be lower than electricity from a traditional LWR [16]. Proliferation resistance can be problematic, and depends on the individual design and operators, but unless there is a possibility of extracting protactinium, it should be as good as or better than in other designs (again, see section 3.3).

There are also a few other less desirable traits, such as the high radiation levels outside the core and the possible release of hydrofluoric acid if the salt comes into contact with water. Compared to the analogous problem in sodium-cooled reactors, however, the latter of these problems should not be seen as particularly troubling. The MSR also has tough material demands; any material used in piping should be able to withstand both chemical attacks

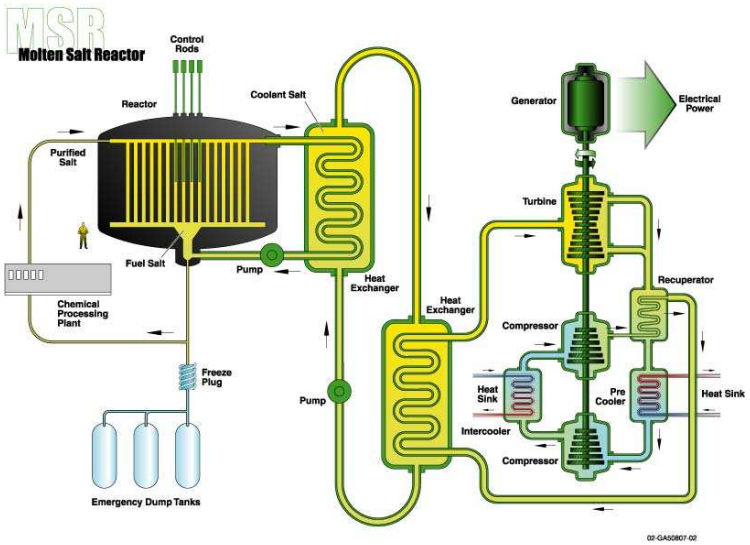

Figure 3.1: Schematic of an MSR from the GIF road map [9].

from the salt and high radioactivity. While Hastelloy N seems to have worked well, there are a few questions regarding the long term stability of it. Furthermore, while the reactor will not have to be stopped for refuelling, the graphite moderator will over time be degraded by radiation and have to be replaced.

Other, non-technical problems lie in licensing – since the design differs so much from traditional reactors, less previous experience can be carried over than for some other novel reactor types – and the fact that since there is no fuel manufacture to profit from, the industry is not as interested in MSRs as in other innovative systems.

3.2 MSR neutronics

An MSR is distinct from a traditional reactor in at least three important ways:

1. Most of the fission energy is released directly into the coolant
2. Due to radiation heating, the graphite moderator is cooled by the fuel salt
3. The delayed neutron precursors are convected with the fuel flow

From a basic neutronics standpoint, the last of these three is the most important, as it directly affects the appropriate equations. The other two are of course of immense importance in any thermohydraulic calculations, but only affect the neutronics indirectly.

The drifting neutron precursors affect both the static and dynamic behaviour of the reactor. In other reactor designs, the precursors stay were they are created – not so in an MSR. This has the disadvantage of making the delayed neutrons on average contribute less to the reactivity of the reactor:

delayed neutrons will inevitably be lost when the precursors decay outside the core, and many of them will also decay at positions of lower importance inside the core than in traditional reactors. This redistribution of delayed neutrons will of course also affect the dynamic properties of the reactor. The consequences of this effect on the dynamics of the MSR will be investigated and analysed in detail in this thesis.

3.3 Thorium fuel

Even if MSRs can run on any fuel, they have attracted special interest as part of a thorium breeder cycle: the online reprossessing possible in MSRs makes them attractive as breeders in general, and the fact that they have better neutron economy than other thermal designs makes them especially attractive for thorium, which has a relatively high thermal absorption cross section. MSRs also avoid the problem that the manufacture of ThO_2 fuel is somewhat more complicated than UO_2 (though ThO_2 does have other advantages).

Apart from the physical and chemical advantages given below, thorium has some other attractive features, such as high abundance in nature – there is estimated to be much more thorium than uranium available[a] – and relatively problem-free mining: the radon daughter nuclide has a shorter half-life than that of uranium, and the mining can be done in open pits, which both reduces the exposure of the miners to radiation. Furthermore, thorium is today an unwanted byproduct when mining rare earth minerals [18].

The result of breeding Th-232 is U-233, which has a low capture cross section and has an η factor (number of neutrons liberated per absorption) of over 2 over a wide energy range, making it an excellent fuel. A thermal breeder should be quite as effective as a fast one, but with the added advantage of being more compact and requiring less of an initial stockpile of U-233 (one fourth of the Pu-239 needed for initial loading of a U-Pu fast breeder) [17].

Also, if U-233 does capture a neutron, it will first become U-234 and then U-235, which is also fissile. This means that a thorium-fuelled reactor will produce very few transuranium actinides, and thus generate very little waste. It will however generate some Pa-231, which is long lived, as well as the usual fission products. The waste produced will only be roughly one percent of that from a U-Pu cycle, which is in turn roughly one percent of that from a once-trough U cycle [17].

U-233 has higher proliferation resistance than other fissile isotopes, mainly because of the small but significant production of U-232, with a half-life of about 70 years and daughter nuclides which emit highly energetic γ-radiation, which makes U-233 very difficult to handle and all but impossible to conceal. The U-233 can still be used to build nuclear devices, but doing so would be far more difficult than with other fissile material – not only because of the U-232

[a] Exactly how much more is impossible to say, but [17] claims that there is four times at much.

content, but because U-233 requires more technical sophistication. Further, the U-233 can easily be made less desirable by addition of U-238. This would in the end lead to some Pu production, but far less than in traditional reactors [19].

However, these barriers can at least be partially overcome when running an MSR: the precursor of U-232, Pa-233, can be removed and allowed to decay, and afterwards the uranium can be separated from the other Pa isotopes. This is mainly an issue with "break-away" states, because it would require control of the reactor for a long period as well as time to allow the Pa-233 to decay, and then the bomb would have to be quickly deployed to avoid the formation of new U-232 from (n,2n) reactions [19]. Further, because of the relatively short half-life of Pa-233, the separation of it on a large basis is so technically complicated as to not be feasible today [20].

As part of their MSBR project, the ORNL calculated a highest possible breeding factor of 1.06 (so that for every fissile atom consumed, on average an excess of 0.06 are produced), which would give a doubling time (the time it takes to double the stockpile of available fuel) of nearly 20 years. This is only if the Pa is extracted however, but then it is the highest possible achievable for a U-233 breeder in a thorium cycle [7].

CHAPTER 4

MSR NEUTRONICS IN ONE-GROUP THEORY

I'm very well acquainted, too, with matters mathematical
I understand equations, both the simple and quadratical
—Gilbert & Sullivan, *The Pirates of Penzance*

This chapter covers one-group theory for MSRs. The diffusion equations are presented, both the forward and the adjoint equations. The static flux and Green's functions are given in analytical form. Comparisons are made with the theory for traditional reactors. Finally, the noise from a propagating perturbation is calculated and compared to similar perturbations in traditional reactors.

4.1 Basic equations

The neutron equations for MSRs are similar to the equations for standard reactors; the fuel velocity will be negligible when compared to the neutron velocity even at thermal conditions, and will thus not affect the neutron flux directly. However, the flow of the fuel will cause a redistribution of the delayed neutron precursors, which will cause a change in the equations.

Here, we shall use one-dimensional diffusion theory with one group of neutrons and one averaged group of neutron precursors; the two-group theory is in many ways similar but will be treated in the next chapter.

To begin with, we need a set of parameters with which to characterise the reactor. The space dimension will be taken to be the z axis, and the core will stretch from $z = 0$ to $z = H$. In most of the calculations, these points will also be the entry and exit points for the fuel. The fuel movement will be modelled using a constant velocity u, which gives a time of passage through the core $\tau_C = H/u$. There will also be a time of passage τ_L in the loop connecting the outlet with the inlet of the core, with an associated length $L = u\tau_L$, which need not have anything to do with any physical length of piping etc. From these we can also write the recirculation time $\tau = \tau_C + \tau_L$ and a total "length"

$T = H + L$.

With this, we can write the equation for the neutron flux as

$$\frac{1}{v}\frac{\partial\phi(z,t)}{\partial t} = D\nabla^2\phi(z,t) + (\nu\Sigma_f(1-\beta) - \Sigma_a(z,t))\,\phi(z,t) + \lambda C(z,t) \quad (4.1)$$

with the normal boundary conditions $\phi(0,t) = \phi(H,t) = 0$.

The equation for the delayed neutron precursors will need an additional term for the convection of neutrons:

$$\frac{\partial C(z,t)}{\partial t} + u\frac{\partial C(z,t)}{\partial z} = \beta\nu\Sigma_f\phi(z,t) - \lambda C(z,t). \quad (4.2)$$

Also, unlike in reactors with stationary or very slow-moving fuel, we will also need separate boundary conditions for the delayed neutron precursors: unlike traditional reactors, where zero neutron flux implies zero precursors, here there will certainly exist some at the exit point at $z = H$, and, unless τ_L is very large, some at the entry $z = 0$. Our boundary condition will thus relate the amount of precursors at $z = 0$ to that at $z = t$ a time τ_L earlier, corrected for the decay that takes place outside the core:

$$C(0,t) = C(H, t-\tau_L)e^{-\lambda\tau_L}. \quad (4.3)$$

We make the customary division of all time-dependent factors into a static and a time-dependent part, and can thus divide the equations into two sets: one for the static flux, and one for the noise. The static equations will be

$$D\nabla^2\phi_0(x) + (\nu\Sigma_f(1-\beta) - \Sigma_a)\phi_0(z) + \lambda C_0(z) = 0 \quad (4.4)$$

$$u\frac{dC_0(z)}{dz} = \beta\nu\Sigma_f\phi_0(z) - \lambda C_0(z). \quad (4.5)$$

As in a traditional system, we will eliminate $C_0(z)$ from the equations. The details of this can be found in Paper I, and the result is

$$\begin{aligned} &D\nabla^2\phi_0(x) + (\nu\Sigma_f(1-\beta) - \Sigma_a)\phi_0(z) \\ &\quad + \frac{\lambda\beta\nu\Sigma_f}{u}e^{-\frac{\lambda z}{u}}\left(\frac{1}{e^{\lambda\tau}-1}\int_0^H e^{\frac{\lambda z'}{u}}\phi_0(z')dz' + \int_0^z e^{\frac{\lambda z'}{u}}\phi_0(z')dz'\right) = 0. \end{aligned} \quad (4.6)$$

Interpretation of the integral terms

The integral terms in the expression for the delayed neutrons can be given a physical interpretation. Following [21], we note that

$$\frac{1}{e^{n\lambda\tau}-1} = \sum_{n=1}^{\infty} e^{-\lambda\tau} \quad (4.7)$$

and that we can write

$$C_0(z) = \frac{\beta\nu\Sigma_f}{u}\left(\sum_{n=1}^{\infty}\int_0^H e^{-\frac{\lambda}{u}(z-z')-n\lambda\tau}\phi_0(z')dz + \int_0^z e^{-\frac{\lambda}{u}(z-z')}dz'\right) \quad (4.8)$$

This makes it clear that while the last term is the contribution of delayed neutrons from the present passing of the core, the first term is the neutrons from all previous passages. The same conclusion can also be arrived by instead starting from the equation for the delayed neutron precursors, but keeping the time dependence. The details of this procedure are found in Paper IV.

4.1.1 General, analytic solution

Equation (4.6) can be solved exactly by a sum of three exponentials[a]:

$$\phi_0(z) = \sum_{n=1}^{3} a_n e^{k_n z} \tag{4.9}$$

where the exponential constants k[b] are solutions to

$$k^3 + \frac{\lambda}{u}k^2 + B_0^2 k + \left(\frac{\lambda}{u}B_0^2 + C\right) = 0 \tag{4.10}$$

where

$$B_0^2 = \frac{\nu\Sigma_f(1-\beta) - \Sigma_a}{D}, \quad C = \frac{\lambda\beta\nu\Sigma_f}{Du}. \tag{4.11}$$

The general solution can also be written as

$$\phi_0(z) = a_1 e^{\alpha z}\sin\beta z + a_2 e^{\alpha z}\cos\beta z + a_3 e^{\gamma z}, \tag{4.12}$$

which allows for a more elegant incorporation of the boundary conditions, but on the other hand is more difficult to derive the criticality condition. Using the exponential form, the criticality condition is

$$\sum_{n=1}^{3} a_n \frac{1}{k_n + \lambda/u}\left(-1 + \frac{1}{e^{\lambda\tau}-1}(e^{(k_n+\lambda/u)H} - 1)\right) = 0. \tag{4.13}$$

Earlier, the only solutions found took the form of Fourier series expansion (see e.g. [22], from which also the material data of Table 4.1 were taken). However, these numerical solutions have been quite good, which Fig. 4.1 demonstrates, showing both a Fourier expansion truncated after ten terms and the exact solution.

The calculations in [22] were made for a small system, with $H = 50$ cm, $L = 100$ cm, where the static flux will be very symmetric, even if the delayed neutron precursor distribution varies with fuel velocity, and to get a clear asymmetry in the static flux, a very high fraction of delayed neutrons was needed. However, for a large system with $H = 300$ cm, $L = 400$ cm, as can be seen in Fig. 4.2, this asymmetry will appear clearly at fuel velocities around 10 cm/s.

[a] Two of the papers were published before this solution was found, and some of the results have been made using a Fourier series expansion instead. The results will, however, be presented in an order that favours internal logic, not the chronology of when they were produced.

[b] Note that these have nothing to do with the k_{eff} eigenvalue

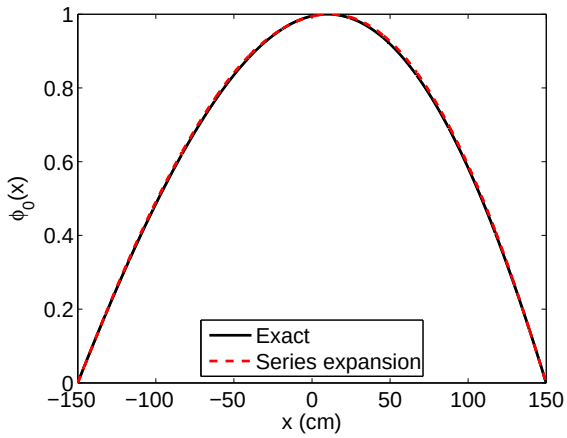

Figure 4.1: Comparison between the exact and the 10 term series expansion solution of the flux. (H=50 cm, $u = 50$ cm/s)

Table 4.1: System parameters representing two uranium-fuelled reactors with different size.

Parameter	Value used
H	50/300 cm
L	100/400 cm
D	0.33 cm
Σ_a	0.01 cm^{-1}
β	0.0065
λ	0.1 s^{-1}

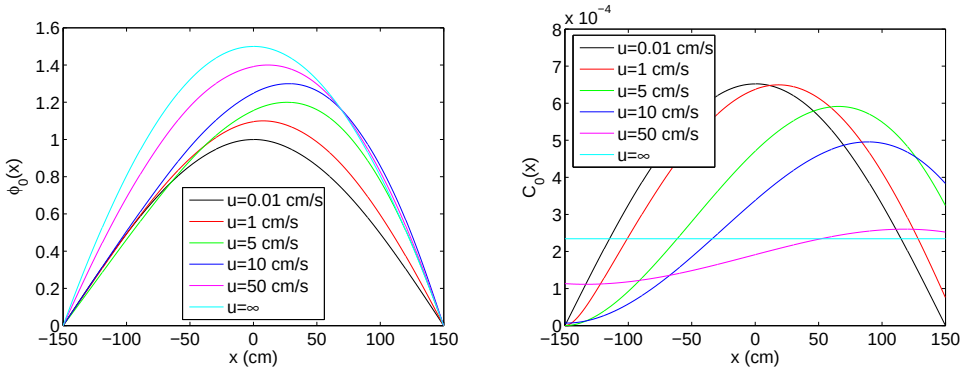

Figure 4.2: Static flux and delayed neutron precursor distribution in the core at various fuel velocities in a large system, $H = 300$ cm.

It should be noted that while the magnitude of the delayed neutron fraction will doubtless be one factor in determining how asymmetric the flux will be, another parameter will be even more so: the diffusion length $L_D = \sqrt{\frac{D}{\Sigma_a}}$. Whether such an asymmetry will be visible in a full-scale system will thus depend on several different parameters. In general, a MSR with a graphite moderator should have rather long diffusion length and thus be nearly symmetric, which will be compounded by the lower value of β in a reactor containing thorium or minor actinides.

4.1.2 Boundary conditions

With an analytical solution, there is more flexibility when choosing boundary conditions. The simplest one is to extrapolate the flux, using the same function outside the physical core as inside it, and demanding that it is exactly zero at some point. While this makes some sense for traditional reactors where the physics outside the proper reactor is of at best secondary interest as long as the physics inside the reactor is modelled accurately, in a MSR, creation and decay of the delayed neutron precursors outside the core will affect the neutronics inside it. Thus, the standard assumption of a flux that vanishes at a certain point and that this point is also where the fuel exits or enters the core is not entirely satisfactory: the mere presence of delayed neutron precursors should ensure that the flux is non-zero.

However, if we try to improve the solution by using logarithmic boundary conditions, so that

$$\phi_0(0) = \ell\phi'(0), \quad \phi_0(H) = -\ell\phi'(H) \tag{4.14}$$

where ℓ is the extrapolation length, and

$$C_0(0) = C_0(H)e^{-\lambda\tau_L} \tag{4.15}$$

and compare it to boundary conditions where the flux is extrapolated and made to vanish at $z = -\ell$ and $z = H + \ell$, and where

$$C_0(-\ell) = C_0(H + \ell)e^{-\lambda\tau'_L}, \tag{4.16}$$

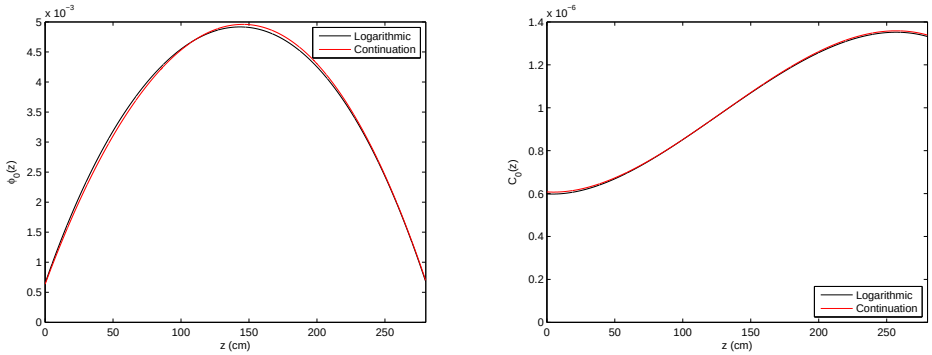

Figure 4.3: Static flux and delayed neutron precursor distribution in the core for two different boundary conditions, $H = 300$ cm.

where

$$\tau_L' = \tau_L - \frac{2\ell}{u}, \tag{4.17}$$

we can see that the differences, while visible, are small (Fig. 4.3). Therefore, we will from now on only be using the boundary condition of zero flux at the extrapolated boundary, as it is in general easier to work with.

4.2 The adjoint

Before moving on to the time dependent equations, we shall first look at the adjoint equations; unlike in one-group theory for reactors with stationary fuel, the equations are not self-adjoint: the flow of the delayed neutron precursors is not invariant under time-reversal.

This property can be easily seen by writing the equations in matrix form:

$$\hat{\mathbb{M}}\vec{\Phi}_0(z) = \begin{pmatrix} D\nabla^2 + \nu\Sigma_f(1-\beta) - \Sigma_a & \lambda \\ -\nu\Sigma_f\beta & u\frac{\partial}{\partial z} + \lambda \end{pmatrix} \begin{bmatrix} \phi_0(z) \\ C_0(z) \end{bmatrix} = 0. \tag{4.18}$$

Because of the first derivative with regards to z in the second row, we find that in general,

$$\left\langle \vec{\Psi}_0(z) | \hat{\mathbb{M}}\vec{\Phi}_0(z) \right\rangle \neq \left\langle \vec{\Phi}_0(z) | \hat{\mathbb{M}}^T\vec{\Psi}_0(z) \right\rangle \tag{4.19}$$

where we have used brackets to indicate integration over the core:

$$\left\langle \vec{\Phi}_0(z) | \vec{\Psi}_0(z) \right\rangle = \int_0^H \vec{\Phi}_0(z)\vec{\Psi}_0(z)dz. \tag{4.20}$$

All terms but the convection term give equal contributions to both sides of (4.19). Since the equation is not self adjoint, we will need to construct an adjoint matrix $\hat{\mathbb{M}}^\dagger$ such that

$$\left\langle \vec{\Phi}_0^\dagger(z) | \hat{\mathbb{M}}\vec{\Phi}_0(z) \right\rangle = \left\langle \vec{\Phi}_0(z) | \hat{\mathbb{M}}^\dagger\vec{\Phi}_0^\dagger(z) \right\rangle. \tag{4.21}$$

Finding $\hat{\mathbb{M}}^\dagger$ is easy; we know that it is similar to $\hat{\mathbb{M}}^T$, but that we shall have to modify the streaming term. Considering the relation of the adjoint to time reversal, we can see that the change should be done by changing the sign of this term, which yields:

$$\hat{\mathbb{M}}^\dagger = \begin{pmatrix} D\nabla^2 + \nu\Sigma_f(1-\beta) - \Sigma_a & -\nu\Sigma_f\beta \\ \lambda & -u\frac{\partial}{\partial z} + \lambda \end{pmatrix}. \tag{4.22}$$

We will also need to change the boundary conditions for the adjoint precursors in a similar manner:

$$C_0^\dagger(0) = C_0^\dagger(H)e^{\lambda\tau_L} \tag{4.23}$$

The proof that this is indeed the adjoint equation can be found in Paper I.

If we now eliminate the adjoint precursors from the equations, similarly to what was done for the normal flux, we will find

$$\begin{aligned} &D\nabla^2\phi_0^\dagger(x) + (\nu\Sigma_f(1-\beta) - \Sigma_a)\phi_0^\dagger(z) \\ &\quad - \frac{\lambda\beta\nu\Sigma_f}{u}e^{\frac{\lambda z}{u}}\left(\frac{1}{e^{-\lambda\tau}-1}\int_0^H e^{-\frac{\lambda z'}{u}}\phi_0(z')dz' + \int_0^z e^{-\frac{\lambda z'}{u}}\phi_0(z')dz'\right) = 0. \end{aligned} \tag{4.24}$$

4.3 Limiting cases

There are three limiting cases of interest for the MSR model: zero fuel velocity, infinite fuel velocity, and no fuel recirculation. The first of these should correspond to a traditional reactor, and is little more than a control that the equations are consistent (see Paper I). The second two are of more interest. They could be potential approximations: if the fuel recirculation time is so short that precursors from previous cycles dominate over the ones from the present cycle, or if it is so long that only the precursors from the present cycle are of importance, then these might be valid models. They could also be useful simplifications, easier to study than the full problem but still giving insight to the physics. They also support the interpretation of the integral terms given in Section 4.1.

The MSR with no recirculation, derived by letting $\tau_L \to \infty$, does not offer very much in terms of simplified equations; there is still an indefinite integral term:

$$\begin{aligned} &D\nabla^2\phi_0(x) + (\nu\Sigma_f(1-\beta) - \Sigma_a)\phi_0(z) \\ &\quad + \frac{\lambda\beta\nu\Sigma_f}{u}e^{-\frac{\lambda z}{u}}\int_0^z e^{\frac{\lambda z'}{u}}\phi_0(z')dz' = 0. \end{aligned} \tag{4.25}$$

This means that the solution will have the same general form with three exponential terms as in the full problem. The equations for the exponential constants k_n will still be the same, but the criticality equation will be simpler:

$$\sum_{n=1}^{3}\frac{A_n}{\lambda/u + k_n} = 0 \tag{4.26}$$

This is not so much of a simplification as to be worth investigating further; the equation is (if the expressions for k_n are written out) still so large that it is practically solvable only by to use computer codes with the capability of handling symbolic algebra, and then the gain over using the more exact equation is greatly diminished.

However, it is still likely to be a good approximation, whose advantaged might be utilised in fully numerical solutions. This is best seen by taking a system with recirculation, making it critical, and then remove the recirculation, and calculate how far from criticality it now is. By then increasing the time in the external loop τ_L, one can get a measure of the error made in assuming no recirculation for different recirculation times. Such a comparison can be seen in Table 4.3, for a system with $H = 300$ cm and $u = 50$ cm/s. As can be seen, it is sufficient for the fuel to spend about a minute in the external loop for the difference to be negligible, and even at a time of half a minute, the reactivity change is only slightly more than a cent.

L (cm)	τ_L (s)	k_{eff}	ρ (\$)
400	8	0.998910	0.168
600	12	0.999343	0.101
800	16	0.999590	0.0631
1000	20	0.999738	0.0403
1200	24	0.999831	0.0260
1400	28	0.999891	0.0168
1600	32	0.999930	0.0108
1800	36	0.999956	0.00677
2000	40	0.999973	0.00415
2200	44	0.999984	0.00246
2400	48	0.999991	0.00138
2600	52	0.999996	0.000615
2800	56	1	0

The case of infinite fuel velocity, in contrast, is probably a more inexact approximation, but is on the other hand a real simplification of the problem, where the equations can be written out explicitly, using only the basic reactor constants, facilitating understanding of the problem. It can also be seen as a limiting case, where the MSR in certain aspects will deviate maximally from the behaviour of the corresponding traditional reactor.

However, in section 4.1 we said that the velocity of the fuel would be so low that the neutronics would not be affected by the relative speed of the neutrons compared to the fuel. This will still be true, as long as we interpret "infinite" in a reasonable way: for a physical reactor, it would mean that the delayed neutron precursor density is constant, i.e. that there is no correlation between where a delayed neutron precursor is created and where it decays. It is not possible to give an exact definition when the reactor can be approximated as acting in such a way, but at $u = 1000$ cm/s, the difference in concentration between the highest and the lowest point is about 5 %, so any reasonable

definition should put the transition point well below the neutron velocity.

Taking the equations to the limit of infinite fuel velocity is easy; the velocity mostly appears in exponentials, turning them into factors of unity, and the $1/u$ in front of the integral from 0 to z causes it to vanish; the only part that needs some work is the product in front of the other integral, but even this poses no real challenge (see Paper I). The equation for the static flux is then

$$D\nabla^2\phi_0(z) + (\nu\Sigma_f(1-\beta) - \Sigma_a)\,\phi_0(z) + \frac{\beta\nu\Sigma_f}{T}\int_0^H \phi_0(z')dz' = 0 \quad (4.27)$$

where $T = H + L$.

This equation, unlike the equations for finite velocity, is self-adjoint, and the system is symmetric around $H/2$ (the same will turn out to be true for the equation for the Green's function). To make better use of this fact, we change the space variable to $x = z - H/2$, so that the system boundaries lies at $x = \pm a$, where $a = H/2$.

The change of coordinates does not affect the equation for the exponential constants k, but taking the limit will, and the equation will now have a form which makes the solutions obvious:

$$k(k^2 + B_0^2) = 0 \quad (4.28)$$

From this, and using the symmetry of the problem and the boundary conditions, we can write the flux as

$$\phi_0(x) = A(\cos B_0 x - \cos B_0 a) \quad (4.29)$$

where

$$B_0^2 = \frac{\nu\Sigma_f(1-\beta) - \Sigma_a}{D}. \quad (4.30)$$

The factor A is arbitrary since the equation is homogeneous, but we still need a condition of criticality. This can be obtained by putting Eq. (4.29) into Eq. (4.27), which gives

$$B_0^2 \cos B_0 a + \frac{2a\eta_0}{T}\cos B_0 a - \frac{2\eta_0}{TB_0}\sin B_0 a = 0 \quad (4.31)$$

where $\eta_0 = \frac{\nu\Sigma_f\beta}{D}$.

4.4 Time dependent equations

We now return to the time dependent problem. The equations will undergo the same modifications as in a traditional reactor, after Fourier transformation: in the neutron equation, an $\frac{i\omega}{v}\delta\phi(x,\omega)$ term will appear, and in the precursor

equation, λ will be replaced by $\lambda + i\omega$. Thus

$$D\nabla^2\delta\phi(z,\omega) + \left(\nu\Sigma_f(1-\beta) - \Sigma_a - \frac{i\omega}{v}\right)\delta\phi(z,\omega) + e^{-\frac{(\lambda+i\omega)z}{u}}\frac{\lambda\beta\nu\Sigma_f}{u}\left(\frac{1}{e^{(\lambda+i\omega)\tau}-1}\int_0^H e^{\frac{(\lambda+i\omega)z'}{u}}\delta\phi(z',\omega)dz' + \int_0^z e^{\frac{(\lambda+i\omega)z'}{u}}\delta\phi(z',\omega)dz'\right) = \delta\Sigma_a(z,\omega)\phi_0(z). \tag{4.32}$$

The general properties of this equation will be investigated using the Green's function technique, i.e. the right hand side will be replaced by $\delta(z - z_p)$, and the equation will be solved for $G(z, z_p, \omega)$ instead of $\delta\phi(z, \omega)$.

We shall start with the simplified case of infinite neutron velocity, which has a solution that can be written out explicitly, making it easier to handle in some analytic manipulations. The equation for the neutron noise in this limit (and with coordinates shifted) is

$$D\nabla^2\delta\phi(x,\omega) + \left(\nu\Sigma_f(1-\beta) - \Sigma_a - \frac{i\omega}{v}\right)\delta\phi(x,\omega) + \frac{\lambda\beta\nu\Sigma_f}{(\lambda+i\omega)T}\int_{-a}^{a}\delta\phi(x',\omega)dx' = \delta\Sigma_a(x,\omega)\phi_0(x) \tag{4.33}$$

For the Green's function $G(x, x_p, \omega)$, we first define

$$B^2(\omega) = B_0^2 - \frac{i\omega}{vD} \tag{4.34}$$

and

$$\eta(\omega) = \frac{\lambda}{\lambda + i\omega}\eta_0. \tag{4.35}$$

This means we can write the equation for the Green's function of Eq. (4.33) as

$$\nabla^2 G(x, x_p, \omega) + B^2(\omega)G(x, x_p, \omega) + \frac{\eta(\omega)}{T}\int_{-a}^{a} G(x', x_p, \omega)dx' = \delta(x - x_p). \tag{4.36}$$

The solution for this will be sought in a similar manner to the solution of the transport equation with a source, where the solution is divided into two parts, one for the uncollided flux and one equation for the collided flux. Here, we shall instead have one term for the behaviour of the flow if there had been no delayed neutrons, i.e. the above equation without the integral term, and one term for all neutrons coming from the delayed neutron precursors, directly or through later fission processes. The former of the terms will be similar to the Green's functions of traditional reactors, the latter will be similar to the expression of the static flux (4.29). The Green's function can thus be written as

$$G(x, x_p, \omega) = A\left(\cos Bx - \cos Ba\right) + \begin{cases} G\sin B(a+x) & x < x_p \\ H\sin B(a-x) & x > x_p \end{cases} \tag{4.37}$$

where $B = B(\omega)$ and A, G and H are functions of x_p and ω but not x.[c] The second term is the same as for a traditional reactor, hence the constants G and H can be determined in the same manner as for such a reactor, yielding

$$H = -\frac{\sin B(a + x_p)}{B \sin 2Ba}; \qquad G = -\frac{\sin B(a - x_p)}{B \sin 2Ba}. \tag{4.38}$$

The remaining constant A can be determined by inserting the expression for the Green's function into Eq. (4.36). Defining

$$K(\omega) = B^2 \cos Ba + \frac{2a\eta(\omega)}{T} \cos Ba - \frac{2\eta(\omega)}{TB} \sin Ba \tag{4.39}$$

and

$$\varphi(x) = \cos Bx - \cos Ba \tag{4.40}$$

we have

$$G(x, x_p, \omega) = \frac{\eta(\omega)\varphi(x)\varphi(x_p)}{TK(\omega)B^2 \cos Ba} - \frac{1}{B \sin 2Ba} \begin{cases} \sin B(a - x_p) \sin B(a + x) & x < x_p \\ \sin B(a + x_p) \sin B(a - x) & x > x_p \end{cases} \tag{4.41}$$

Note that $K(0) = 0$, as this is the criticality equation. Also, it is the first term of the above equation containing $K(\omega)$, not present in a traditional reactor, which is responsible for the point-kinetic behaviour of the reactor at low frequencies. Normally, what is here the second term would determine the behaviour of the reactor over all frequencies, but that term will remain finite here even at $\omega = 0$, since the factor $\sin 2Ba$ in the denominator does not tend to zero when $\omega \to 0$. For low frequencies, we thus have

$$G(x, x_p, \omega) \sim \frac{\eta_0 \varphi(x)\varphi(x_p)}{TK(\omega)B_0^2 \cos B_0 a} \tag{4.42}$$

Since it is thus possible to factorise the Green's function into frequency and space dependence, and the space dependence can be written as a product of the static flux at x and x_p, the MSR also shows point-kinetic behaviour at low frequencies.

Comparison with a traditional reactor

While the expression of the Green's function for a MSR is different from that of a traditional reactor, this does not in itself mean that the behaviour must be very different. To truly get an idea what, if anything, makes them different, it is necessary to do a quantitative comparison.

Some system parameters for a uranium fuelled reactor can be found in Table 4.1, taken from [22]. Other important parameters, such as $\nu\Sigma_f$, will

[c] The temporary constant H should not be confused with the reactor height H

differ somewhat between the two reactor types if they are to have the same physical size.

The Green's function of a traditional reactor is

$$G(x, x_p, \omega) = -\frac{1}{B'(\omega)\sin 2B'(\omega)a} \begin{cases} \sin B'(\omega)(a+x)\sin' B(\omega)(a-x_p) & x \leq x_p \\ \sin B'(\omega)(a-x)\sin B'(\omega)(a+x_p) & x > x_p \end{cases} \tag{4.43}$$

where

$$(B'(\omega))^2 = (B_0')^2 \left(1 - \frac{1}{(1-\frac{\Sigma_a}{\nu\Sigma_f})G_0(\omega)}\right), \tag{4.44}$$

$$G_0(\omega) = \frac{1}{i\omega\left(\Lambda + \frac{\beta}{i\omega+\lambda}\right)} \tag{4.45}$$

and $B_0' = \pi/H$.

Fig. 4.4, showing the space dependence of the absolute value of the Green's function at $x_p = 0$ and different frequencies for a large reactor of height $H = 300$ cm, reveals several interesting features: at low frequencies, the two functions have the same shape, but the MSR Green's function has a much larger amplitude. As the frequency increases, this difference in amplitude decreases, but at the same time, the change in shape from the cosine structure at low frequencies to a more localised, tent-like shape is somewhat different: this happens faster in the traditional reactor than in the MSR. At very high frequencies, where the behaviour is independent of the delayed neutron precursors, finally, the Green's functions for the two reactor types have the same shape and amplitude.

The difference in amplitude can be explained from the fact that the delayed neutron economy is worse in the MSR. For a traditional reactor, it can be shown that for medium and low frequencies, $G \propto 1/\beta$. Even if the nuclear constant β is the same in the two reactors, the MSR will operate with an effective fraction of delayed neutrons β_{eff} smaller than β, since the precursors decays both outside the core and at positions with lower importance inside the core than in a traditional reactor. If we neglect the second effect and focus only on the neutrons that are lost due to decay outside of the core, we can get an estimate for β_{eff} as follows:

$$\beta_{eff} \approx \beta \frac{\tau_H}{\tau_H + \tau_L} \tag{4.46}$$

For a reactor with $H = 300$ and $L = 400$, this means that the Green's function should be about 2.3 times larger than that of its traditional counterpart. This estimate can be compared to Figs. 4.4(a) and 4.4(b), which shows a similar ratio.

This difference in amplitude is expected to be even larger in any real MSR, which will run on fuel with a smaller fraction of delayed neutrons. This means

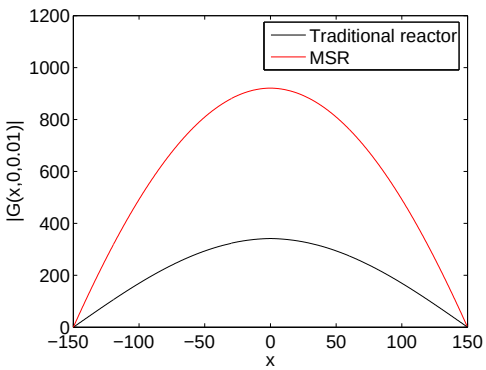

(a) $\omega = 0.001$ rad/s

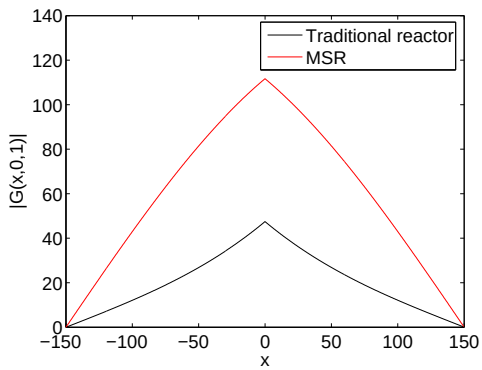

(b) $\omega = 1$ rad/s

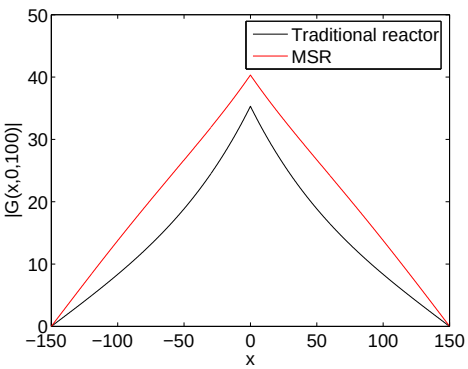

(c) $\omega = 100$ rad/s

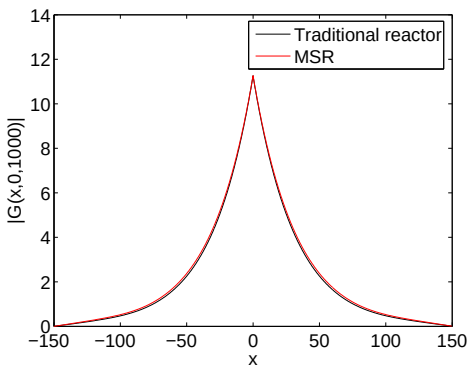

(d) $\omega = 1000$ rad/s

Figure 4.4: Comparison between Green's functions for infinite and zero fuel velocity for various frequencies in a large system ($H = 300$ cm). (a) $\omega = 0.001$; (b) $\omega = 1$; (c) $\omega = 100$; (d) $\omega = 1000$ rad/s.

a larger amplitude of the noise level for the same strength of the noise source, which fact will make noise analysis an even more valuable and suitable tool in such reactors.

The difference in shape, where the MSR retains the point-kinetic shape at higher frequencies, is a sign that the MSR is more tightly coupled than the traditional reactor. This is due to two differences: the transport of delayed neutron precursors from one region of another will be a rather weak but far-reaching coupling. More important, however, is that since the prompt neutrons will also be of higher importance, the prompt neutron chains will be longer and further increase the coupling. Together these two effects ensure that an MSR will be more tightly coupled than a traditional reactor of the same physical size.

The point kinetic component

Trying to find the point kinetic component of a reactor with infinite fuel velocity is illuminating some of the problems with the mathematics of the MSR; a similar investigation could be done of the general problem, but the problems are fundamentally the same and the simpler expressions in the infinite limit makes them clearer.

First, we note that we can, at low frequencies, use Eq. (4.42) to write an asymptotical zero-power transfer function

$$G_0(\omega)^{Asy.} = -\frac{\eta(\omega)\nu\Sigma_f}{TK(\omega)B^2(\omega)\cos B(\omega)a}. \tag{4.47}$$

However, it turns out that this does not encode all of the point kinetic behaviour; the term in Eq. (4.41) that was neglected also has components that show point kinetic behaviour. To obtain these, it is necessary to take the projection of the full Green's function on to the static flux, i.e. to calculate

$$\delta P(\omega) \equiv \frac{\int_{-a}^{a} \delta\phi(x,\omega)\phi_0(x)dx}{\int_{-a}^{a} \phi_0^2(x)dx} \tag{4.48}$$

In the asymptotic limit, it is easy to find a general expression

$$\delta P(\omega)^{Asy.} = G_0(\omega)^{Asy.}\rho(\omega) \tag{4.49}$$

where

$$\rho(\omega) = -\frac{\int_{-a}^{a} \delta\Sigma_a(x,\omega)\phi_0^2(x)dx}{\nu\Sigma_f \int_{-a}^{a} \phi_0^2(x)dx}. \tag{4.50}$$

However, we cannot derive such a simple solution in the general case; instead we shall have to multiply Eq. (4.36) with the static flux and integrate (doable, but the resulting expressions are hardly compact), or we shall have to derive something using the fact that the noise is known.

The path one would traditionally follow to obtain $\delta P(\omega)$ would be to start with the equations for the static flux and the noise, multiply the former with $\delta\phi(x,\omega)$ and the latter with $\phi_0(x)$, integrate the equations over the reactor core and take the difference. Writing $\delta\phi(x,\omega) = P(\omega)\phi_0(x) + \delta\psi(x,\omega)$ and using the fact that $\phi_0(x)$ and $\delta\psi(x,\omega)$ are orthogonal, the end result would then be an equation where $\delta\phi(x,\omega)$ is dropped and a simple expression for $P(\omega)$ is found. Doing the same with Eq. (4.27) and (4.33), however, but keeping $\delta\phi(x,\omega)$, yields

$$\frac{i\omega}{v}\int_{-a}^{a}\delta\phi(x,\omega)\phi_0(x)dx + \frac{i\omega}{i\omega+\lambda}\frac{\beta\nu\Sigma_f}{T}\int_{-a}^{a}\delta\phi(x,\omega)dx\int_{-a}^{a}\phi_0(x)dx = -\int_{-a}^{a}\delta\Sigma_a(x,\omega)\phi_0^2(x)dx. \tag{4.51}$$

This is more complicated to handle than the corresponding equation for the traditional reactors because of the second term: instead of an integral where the integrand is a product of the static flux and the noise, we now have a product of two integrals where one has the static flux and the other the noise as integrands.

The first term is equivalent to $\delta P(\omega)$, so if we can evaluate the other terms, we are set. First, we introduce some new notation:

$$\phi_0(x,\omega) = A\left(\cos B(\omega)x - \cos B(\omega)a\right), \tag{4.52}$$

$$\varphi_0(x,\omega) = \cos B(\omega)x - \cos B(\omega)a. \tag{4.53}$$

Note that

$$\phi_0(x,0) = \phi_0(x), \tag{4.54}$$

$$\varphi_0(x,0) = \varphi_0(x). \tag{4.55}$$

Now, we rewrite

$$\int_{-a}^{a}\delta\phi(x,\omega)dx = \frac{1}{D}\int_{-a}^{a}\int_{-a}^{a}G(x,x_p,\omega)\delta\Sigma_a(x_p,\omega)\phi_0(x_p)dx_pdx \tag{4.56}$$

using the fundamental quality of the Green's function. We note that this new integral can be written as

$$\int_{-a}^{a}\int_{-a}^{a}G(x,x_p,\omega)\delta\Sigma_a(x_p,\omega)\phi_0(x_p)dx_pdx = \int_{-a}^{a}\left(\int_{-a}^{a}G(x,x_p,\omega)dx\right)\delta\Sigma_a(x_p,\omega)\phi_p(x_p)dx_p \tag{4.57}$$

The inner integral can be evaluated using Eq. (4.36):

$$\int_{-a}^{a}G(x,x_p,\omega)dx = -\frac{\cos B(\omega)x_p - \cos B(\omega)a}{K(\omega)} \equiv -\frac{\phi_0(x_p,\omega)}{K(\omega)}. \tag{4.58}$$

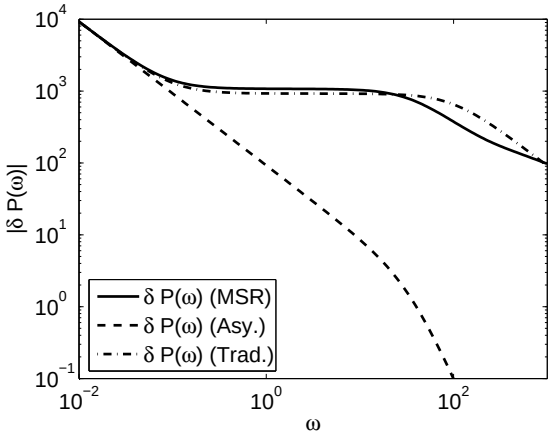

Figure 4.5: Frequency dependent part of the point kinetic term, for MSR and corresponding traditional reactor.

We can now turn to the term we originally wanted to evaluate:

$$\begin{aligned}
&\int_{-a}^{a} \delta\phi(x,\omega)dx \int_{-a}^{a} \phi_0(x)dx \\
&= -\frac{1}{DK(\omega)} \int_{-a}^{a} \varphi_0(x,\omega)\delta\Sigma_a(x,\omega)\phi_0(x)dx \int_{-a}^{a} \phi_0(x)dx \\
&= -\frac{1}{DK(\omega)} \int_{-a}^{a} \phi_0(x,\omega)\delta\Sigma_a(x,\omega)\phi_0(x)dx \int_{-a}^{a} \varphi_0(x)dx. \qquad (4.59)
\end{aligned}$$

The last of these integrals can be directly evaluated by using Eq. (4.27) and (4.31)

$$\int_{-a}^{a} \varphi_0(x)dx = \frac{2}{B_0}\sin B_0 a - 2a\cos B_0 a = \frac{T}{\eta_0}B_0^2 \cos B_0 a. \qquad (4.60)$$

We now define

$$\rho'(\omega) = -\frac{\int_{-a}^{a} \delta\Sigma_a(x,\omega)\phi_0(x)\phi_0(x,\omega)dx}{\nu\Sigma_f \int_{-a}^{a} \phi_0^2(x)dx}, \qquad (4.61)$$

and can thus go back to Eq. (4.51), and divide it by $\nu\Sigma_f \int_{-a}^{a} \phi_0^2(x)dx$. This yields

$$\frac{i\omega}{v\nu\Sigma_f}\delta P(\omega) + \frac{i\omega}{i\omega+\lambda}\frac{\beta\nu\Sigma_f}{T}\rho'(\omega)\frac{1}{DK(\omega)}\frac{T}{\eta_0}B_0^2\cos B_0 a = \rho(\omega) \qquad (4.62)$$

and thus

$$\delta P(\omega) = \frac{1}{i\omega\Lambda}\left(\rho(\omega) - \frac{i\omega}{i\omega+\lambda}\frac{B_0^2\cos B_0 a}{K(\omega)}\rho'(\omega)\right). \qquad (4.63)$$

The modified reactivity, $\rho'(\omega)$, is similar to the real reactivity only at low frequencies, when $B(\omega) \approx B_0$ and thus also $\phi_0(x,\omega) \approx \phi_0(x)$. For this reason,

the amplitude of the noise cannot be factorised into traditional reactivity and a zero power transfer function, except for asymptotically at low frequencies. Fig. 4.5 is a comparison between the asymptotic solution, the exact solution for a MSR, and the exact solution for a traditional reactor.

4.4.1 Finite velocity

For finite velocities, it is still possible to find closed-form analytical solutions, but they are more complicated than before: it is now solved formally in two regions, where in each it is a sum of three exponential functions, making six different equations for determining the constants necessary: two boundary conditions and two interface conditions, similar to traditional reactors, and two equations that are similar to the criticality condition. This means that the fundamental problem is a 6×6 matrix equation.

However, one can also get some physical insight by using a method first devised to construct a semi-analytical solution, based on how the solution for infinite velocity was found. This was necessary due to the unsuitability to use a pure Fourier series expansion except at low frequencies. At high frequencies, where the strongly local behaviour was seen in both the traditional reactor and the MSR with an infinite fuel velocity, the series expansion will need many terms to converge, and before it has done so, will show several ripples, where the true solution should have a second derivative with the same sign everywhere except at $z = z_p$ (where it should be undefined).

Here, the Green's function will be split into two parts

$$G(z, z_p, \omega) = G_i(z, z_p, \omega) + G_h(z, z_p, \omega) \tag{4.64}$$

where G_i will satisfy the equation

$$D\nabla^2 G_i(z, z_p, \omega) + \left((1-\beta)\nu\Sigma_f - \Sigma_a - \frac{i\omega}{v} \right) G_i(z, z_p, \omega) = \delta(z - z_p). \tag{4.65}$$

It will thus take care of the inhomogeneity, but not the contributions from delayed neutrons. This division into parts is equivalent to what was done for the infinite fuel velocity case, and it will have the same solution as Eq. (4.43), except with B instead of B'.

The remainder G_h will thus take care of any contributions from the delayed neutrons, both the delayed neutrons themselves as well as the fission processes

they will initiate; the equation for it will have the form

$$
\begin{aligned}
&D\nabla^2 G_h(z,z_p,\omega) + \left(\nu\Sigma_f(1-\beta) - \Sigma_a - \frac{i\omega}{v}\right) G_h(z,z_p,\omega) \\
&\quad + e^{-\frac{(\lambda+i\omega)z}{u}} \frac{\lambda\beta\nu\Sigma_f}{u}\left(\frac{1}{e^{(\lambda+i\omega)\tau}-1}\int_0^H e^{\frac{(\lambda+i\omega)z'}{u}} G_h(z',z_p,\omega)dz'\right. \\
&\quad \left. + \int_0^z e^{\frac{(\lambda+i\omega)z'}{u}} G_h(z',z_p,\omega)dz'\right) \\
&= - e^{-\frac{(\lambda+i\omega)z}{u}} \frac{\lambda\beta\nu\Sigma_f}{u}\left(\frac{1}{e^{(\lambda+i\omega)\tau}-1}\int_0^H e^{\frac{(\lambda+i\omega)z'}{u}} G_i(z',z_p,\omega)dz'\right. \\
&\quad \left. + \int_0^z e^{\frac{(\lambda+i\omega)z'}{u}} G_i(z',z_p,\omega)dz'\right). \qquad (4.66)
\end{aligned}
$$

The details of solving this are given in Paper I; suffice to say that it involves solving matrix equations but that the technique is similar to what has to be done if one uses one Fourier series expansion of the whole Green's function, so while the semi-analytical method makes for longer expressions, it does not increase the needed computer power much.

Numerical results can be seen in Figs. 4.6 and 4.7; note that these use different system sizes. Fig. 4.6 shows the frequency dependence in a small system. As can be seen, $G_0(\omega)$ has two separate regions where the solution behaves as $1/\omega$ with one plateau region in between. The amplitude at the plateau increases with increasing fuel velocities, as is to be expected with the decreasing value of β_{eff}. At certain frequencies, peaks nearly one order of magnitude higher than the normal amplitudes can also be seen. These correspond to the inverse of the recirculation time τ, or multiples of the inverse, and thus move to higher frequencies with higher fuel velocity. Their physical meaning should thus be clear; but we can not expect to see them as strongly in a real MSR, where τ_L is likely longer and at best an average quantity.

Fig. 4.7 shows the space and velocity dependence of the absolute value of the Green's function for a large system with $z_p = H/2$ and $\omega = 10$ rad/s, which is located in the middle of the plateau region, for several different fuel velocities. As can be seen, with higher velocities, the amplitude increases, and the shape becomes more and more point-kinetic; the function goes from being convex for $u = 0$ (i.e. a traditional reactor) to concave for $u = \infty$. As has already been mentioned, this is due to the loss of delayed neutrons and the increased neutronic coupling, respectively.

One thing that can be noted is that the earlier assertion of infinite fuel velocity as a limiting case is not strictly true: apart from the asymmetry of the static flux at mid-velocities, there is also a non-monotonic dependence of the magnitude of the Green's function at frequencies below the plateau region.

For such low frequencies, the behaviour of the Green's function is domi-

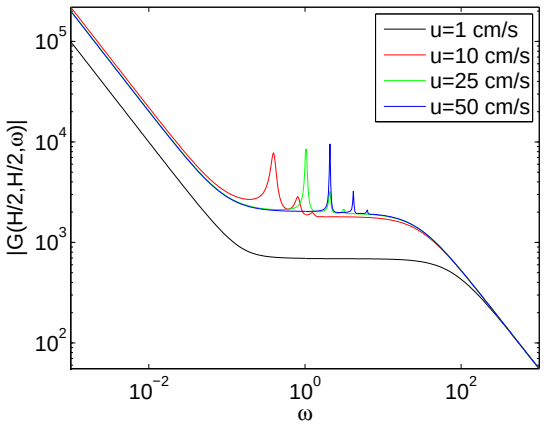

Figure 4.6: Frequency dependence of the Green's function for a few different fuel velocities. $H = 50$ cm, $L = 100$ cm

nated by the contribution from the delayed neutrons, i.e. the terms

$$e^{-\frac{z(\lambda+i\omega)}{u}}\frac{\lambda\beta\nu\Sigma_f}{u}\left(\frac{1}{e^{(\lambda+i\omega)\tau}-1}\int_0^H e^{\frac{(\lambda z'+i\omega)}{u}}G(z',z_p,\omega)dz' + \int_0^z e^{\frac{(\lambda+i\omega)z'}{u}}G(z',z_p,\omega)dz'\right) \tag{4.67}$$

The velocity u affects this in four different ways:

- Through the cross section $\nu\Sigma_f$, which is adjusted to reach criticality. However, a higher fuel velocity means worse neutron economy, which means that the cross section increases monotonically with higher velocity.
- Through the factor $\frac{1}{u\left(e^{\frac{\lambda T}{u}}-1\right)}$ multiplying the first integral. However, this also increases monotonically with u
- Through the $1/u$ factor multiplying the second integral. This would lead to a monotonic decrease.
- Through the exponential terms under the integral signs.

Closer investigation of the behaviour of the corresponding terms in the static equation suggests that it is in fact the last of these, and specifically the phase factor $e^{\frac{i\omega z}{u}}$ that seems to be the most likely source: while the $1/u$ factor also makes at least part of the expression decrease with increasing velocity, the increase of the other term compensate (at least at zero frequency). Thus, the more rapid changes in phase from the higher velocity seem to be the dominant factor.

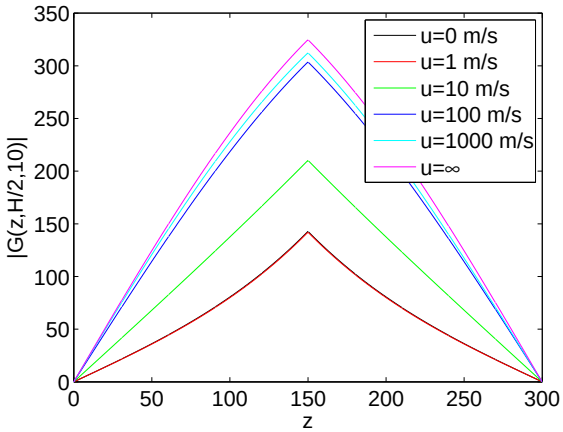

Figure 4.7: Green's function space dependence for some different velocities. Analytical solution for $u = 0$ and $u = \infty$. $H = 300$ cm, $\omega = 10$ rad/s.

4.5 Noise induced by propagating perturbations

One of the differences between an MSR and a traditional reactor is the larger potential of a propagating perturbation. Such things are of course not inconceivable in traditional reactors either, where fluctuations in for example inlet temperature of the coolant can have similar effects, but since such fluctuations in traditional reactors will only affect the coolant but not the fuel as in a MSR, the effects are expected to be stronger in the latter. Also, as has been demonstrated, the Green's functions of MSRs are different from those of traditional reactors, which gives even more incentive to the study.

A propagating perturbation in the absorption cross section can be represented as

$$\delta\Sigma_a(z,t) = \delta\Sigma_a(0, t - z/u) \tag{4.68}$$

or, in the frequency domain,

$$\delta\Sigma_a(z,\omega) = e^{-i\omega z/u}\delta\Sigma_a(0,\omega). \tag{4.69}$$

Since $\delta\Sigma_a(0,t)$ is considered a white noise process, the frequency dependence of its auto-spectrum is constant, and it is possible to without contradiction chose $\delta\Sigma_a(0,\omega) = 1$.

For a traditional reactor in the point-kinetic approximation, the reactivity effect of such a perturbation is

$$\rho(\omega) = -\frac{\int \phi_0^2(z)\delta\Sigma_a(z,\omega)dz}{\nu\Sigma_f \int \phi_0^2(z)dz}. \tag{4.70}$$

In a homogeneous reactor, $\phi_0(z) = \sin\frac{\pi z}{H}$, and

$$\rho(\omega) \propto \frac{\omega_\tau^3}{\pi(\omega_\tau^2 - \omega^2)} e^{\frac{-i\omega\tau_C}{2}} \sin\frac{\omega\tau_C}{2} \tag{4.71}$$

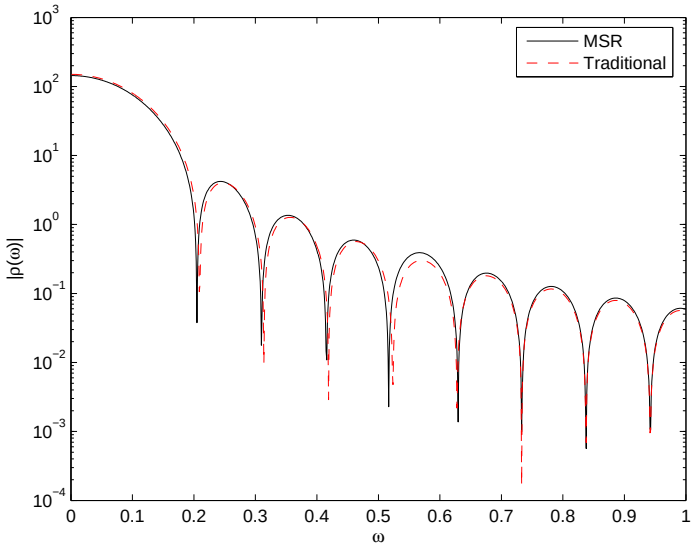

Figure 4.8: Magnitude of the reactivity $\rho(\omega)$ in a one-group MSR; H=300, u=5 cm/s

where $\omega_\tau = \frac{2\pi}{\tau_C}$. This has a characteristic, periodic sink structure, with zeros (which in a lin-log plot show up as sinks) at

$$\omega = \frac{2\pi u}{H} n, \quad n = 2, 3, \ldots \tag{4.72}$$

However, the above is based on the assumption that the equations are self-adjoint; this is certainly not true for the MSR, and the equation must be rewritten as

$$\rho(\omega) = -\frac{\int \phi_0(z)\phi_0^\dagger(z)\delta\Sigma_a(z,\omega)dz}{\nu\Sigma_f \int \phi_0(z)\phi_0^\dagger(z)dz}. \tag{4.73}$$

In a homogeneous MSR, $\phi_0^\dagger(z) = \phi_0(H-z)$, and the integrals are readily calculated. A comparison between a traditional reactor and a MSR at $u = 5$ cm/s (where the flux is clearly asymmetric) can be seen in Figs. 4.8 and 4.9. The behaviour is similar, and we can expect "classical" point-kinetic approximation to work just as well in MSRs as in traditional reactors.

If we want the exact expression for the noise, we shall have to use the Green's function instead. The noise will then be

$$\delta\phi(z,\omega) = \int_0^H G(z, z_p, \omega) e^{-i\omega z_p/u} \phi_0(z_p) dz_p \tag{4.74}$$

which can be readily calculated with the help of the expressions derived for the Green's function and the static flux.

The noise in a small system (Fig. 4.10), is expected to have point-kinetic-like behaviour up to large frequencies, even if the result will be slightly different

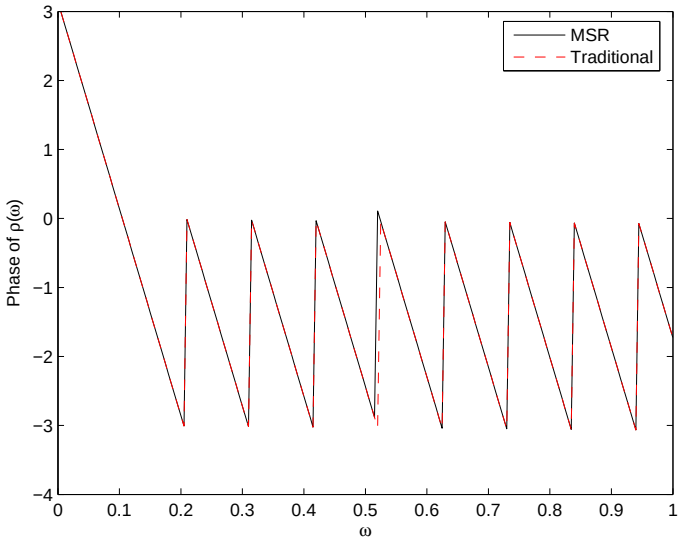

Figure 4.9: Phase of the reactivity $\rho(\omega)$ in a one-group MSR; H=300, u=5 cm/s

from that of a traditional reactor due to the changes in the Green's function: the amplitude is larger than expected, and the peaks in the plateau region clearly show for low frequencies.

For a large system (Fig. 4.11), the behaviour is different: we again have a periodic structure, but there are no zeros, and the periodic structure is different in different parts of the reactor. That the sink structure disappears can be explained by the appearance of contributions to the Green's function and thus the noise other than the point-kinetic; these contributions will not have the sink structure, and depending on the relative strength, it can either mask the point-kinetic contribution entirely, or, as here, make it appear as an oscillation, but one with an amplitude smaller than the average value of the reactivity.

Furthermore, unlike the point-kinetic part, which has a simple phase of $-\omega a/u$, with jumps of π at the sinks, these extra terms will have a rather complicated phase, dependent on both location and frequency, and can be both in-phase and out of phase compared to the point-kinetic part, with the exception of the centre of the reactor, where the symmetry ensures a more predictable behaviour.

This is made clearer by looking at the space dependence of the noise (Fig. 4.12). At low frequencies ($\omega = 1$ rad/s), the noise is point-kinetic, with the cosine shape of the static flux. At $\omega = 7$ rad/s, we see a marked difference; the noise no longer has a maximum in the centre of the core and it is slightly asymmetric. The latter is also a feature of the static flux, but that has a single local maximum. At $\omega = 10$ rad/s, we have three local maxima, and two local minima. This is despite the fact that both the point-kinetic and the space-dependent terms are cosine-shaped when taking the absolute value. Again, it is the phase that is important, and as it is constant for the point

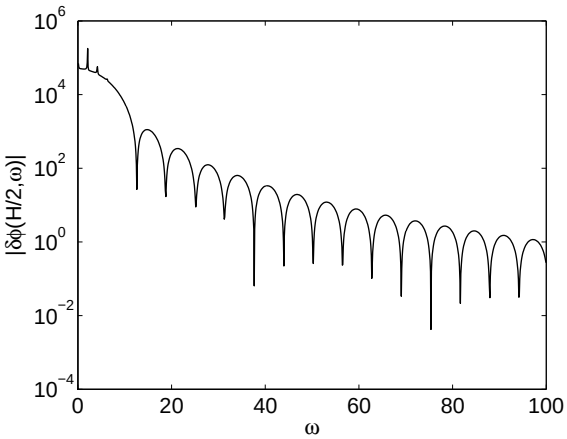

Figure 4.10: The frequency dependence of the amplitude of the neutron noise induced by a propagating perturbation in a small system (H=50 cm, u = 50 cm/s)

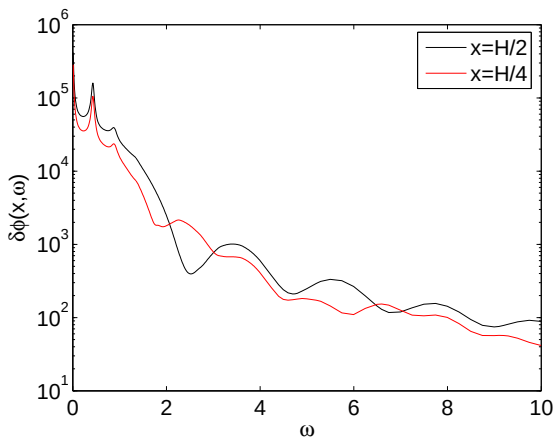

Figure 4.11: The frequency dependence of the neutron noise induced by a propagating perturbation in two different points in a large system (H=300 cm, u = 150 cm/s).

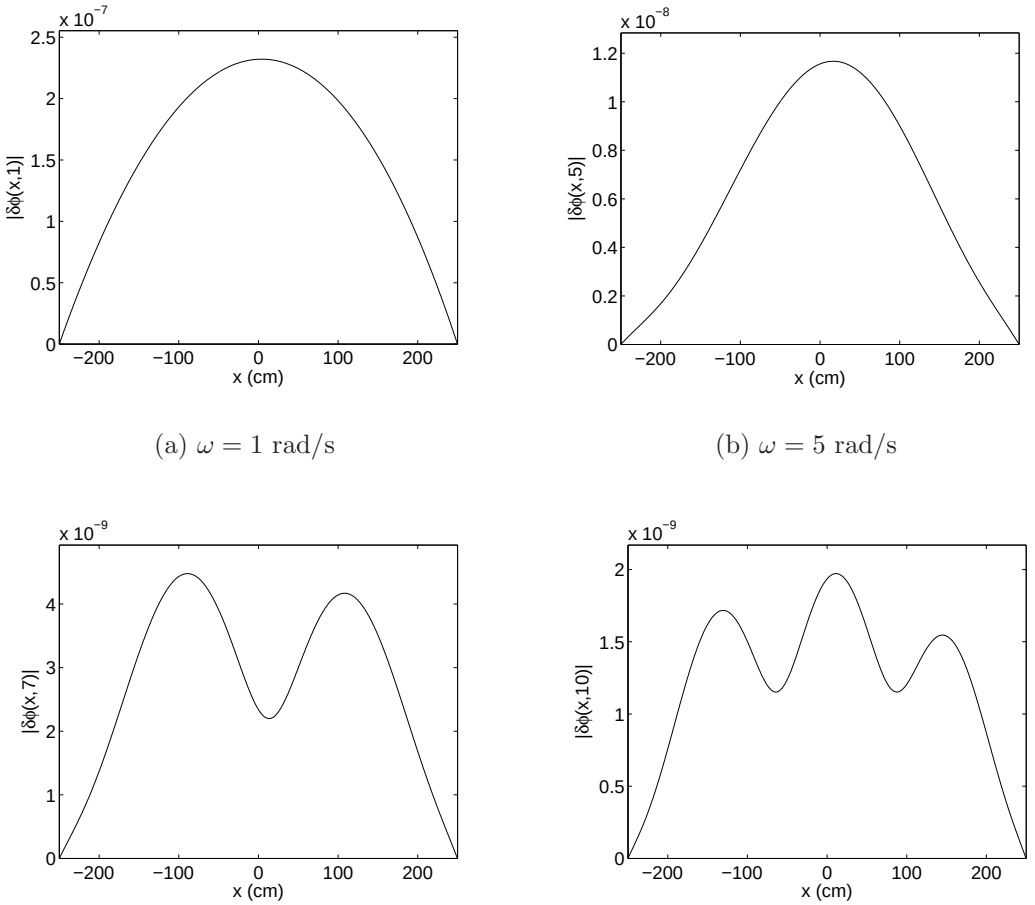

(a) $\omega = 1$ rad/s

(b) $\omega = 5$ rad/s

(c) $\omega = 7$ rad/s

(d) $\omega = 10$ rad/s

Figure 4.12: Comparison between the neutron noise space dependence for different frequencies in a large system ($H = 500$ cm, $v = 250$ cm/s). (a) $\omega = 1$; (b) $\omega = 5$; (c) $\omega = 7$; (d) $\omega = 10$ rad/s.

kinetic term but varying for the space dependent, there will be maxima when the phases are the same and minima when they are opposite.

This behaviour is not seen at low frequencies, because there the space-dependent phase varies more slowly, at the same time as the point-kinetic term dominates the total behaviour. With increasing frequency, the noise will again become smoother, as the space-dependent term will start to dominate instead.

Comparing to a traditional reactor, one finds that there, the oscillating behaviour starts and is diminished at lower frequencies than in a MSR. This is consistent with the previous conclusion that MSRs behave in a more point-kinetic-like manner than traditional reactors.

CHAPTER 5

MSR NEUTRONICS IN TWO-GROUP THEORY

o denna anhopning av siffror och formler, denna härsmakt av symboler uppställda i rader och kolonner och matriser, och se dessa diagram, dessa kurvor, sällsamma projektioner av verkligheten, en bild av tillvaron abstraherad till en enda linje.
—Willy Kyrklund, "Katten", *Den överdrivne älskaren*

This chapter covers two-group theory for MSR. The diffusion equations, both in forward and adjoint form, are presented. The static flux and Green's functions are given in analytical form in the limit of infinite fuel velocity, and the static flux and adjoint Green's functions in semi-analytical form for finite fuel velocity. Three different reactor types are investigated: a thermal, thorium-fuelled reactor, a uranium-fuelled BWR, and a MOX-fuelled fast reactor.

5.1 Investigated systems

In the previous chapter, a simple, uranium-fuelled reactor was used for all calculations, in order to focus on the differences between MSRs and traditional reactors. Here, we shall instead try to see what the difference might be between a more realistic MSR system and existing reactors.

This will be done in two parts:

- For the MSR, three systems will be investigated: a thermal, thorium-fuelled system designed as a realistic MSR, a conventional light-water reactor, based on Ringhals-1, hereafter referred to only as "BWR", and a high conversion reactor concept with a fast spectrum. To reduce the number of cases, all systems will be of a power reactor size. The material and geometrical data for these systems are given in Table 5.1.

Table 5.1: System parameters representing a thorium-fuelled reactor at 550° C, a BWR, and a high conversion U-loaded fast core.

Parameter	Thorium	BWR	Fast
H	300 cm	365.76 cm	300 cm
L	400 cm	400 cm	400 cm
D_1	0.90485 cm	1.7362 cm	1.4719 cm
D_2	0.76445 cm	0.39860 cm	0.53642 cm
Σ_1	0.004806 cm^{-1}	0.0221249 cm^{-1}	0.016835 cm^{-1}
Σ_{a2}	0.003384 cm^{-1}	0.0552976 cm^{-1}	0.28178 cm^{-1}
Σ_R	0.003857 cm^{-1}	0.013782 cm^{-1}	0.0082208 cm^{-1}
β	0.003036	0.00576	0.004
λ	0.0649 s^{-1}	0.0846 s^{-1}	0.086 s^{-1}
v_1	$1.6090570 \cdot 10^8$ cm/s	$1.38308 \cdot 10^9$ cm/s	$5.0806 \cdot 10^7$ cm/s
v_2	$5.57344430 \cdot 10^6$ cm/s	$1.09342 \cdot 10^6$ cm/s	$2.8216 \cdot 10^5$ cm/s

- In order to better understand what effects the moving fuel has, a study of propagating noise in traditional reactors has been made. Results for the reactors that closest resemble those above will be given here.

5.2 Comparison with traditional reactors

Before turning to the actual noise in the MSR, we shall consider the analogous problem in traditional reactors. The theory behind is mostly well known: the equations are very similar to those for the MSR that will be presented later in this chapter, and will not be repeated here; see Paper VI for details. However, the solutions will be covered here briefly.

First, the static flux can be written as

$$\vec{\phi}_0(z) = A \begin{bmatrix} 1 \\ c_\mu \end{bmatrix} \sin B_0 z \tag{5.1}$$

where $c_\mu = \frac{\Sigma_R}{\Sigma_{a2}+D_2 B_0^2}$ and $B_0 = \pi/H$.

The Green's function will consist of four components, $G_{ij}(z, z', \omega)$, where j denotes the source region and i the noise region – i.e. G_{21} is used when there is a fast source and one wants the thermal noise.

The Green's functions can be written

$$\begin{aligned} G_{ij}(x, x_p, \omega) = &\frac{A_{ij}(\omega)}{\mu \sin 2\mu a} \begin{cases} \sin\mu(a-x_p)\sin\mu(a+x) & x < x_p \\ \sin\mu(a+x_p)\sin\mu(a-x) & x > x_p \end{cases} \\ &+ \frac{B_{ij}(\omega)}{\nu \sinh 2\nu a} \begin{cases} \sinh\nu(a-x_p)\sinh\nu(a+x) & x < x_p \\ \sinh\nu(a+x_p)\sinh\nu(a-x) & x > x_p \end{cases} \end{aligned} \tag{5.2}$$

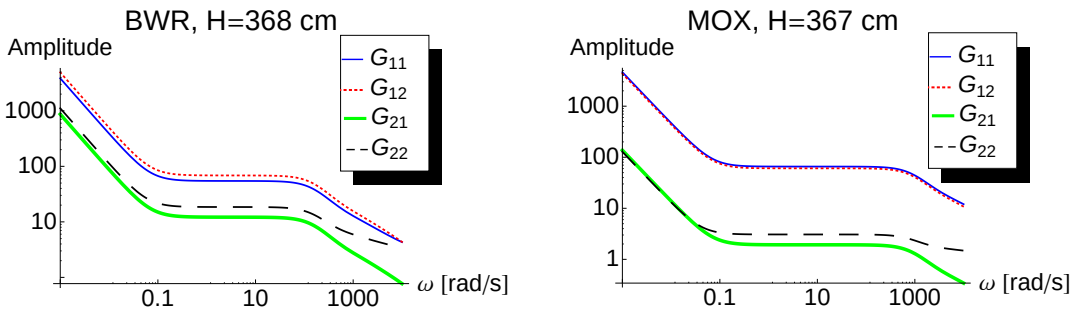

(a) BWR

(b) Fast

Figure 5.1: Frequency dependence of the Green's functions for traditional reactors.

where $\mu = \mu(\omega)$ and $\nu = \nu(\omega)$ are the roots of

$$\left(D_1\mu^2 + \Sigma_1(\omega)\right)\left(D_2\mu^2 + \Sigma_2(\omega)\right) - \nu\Sigma_f(\omega)\Sigma_R = 0 \tag{5.3}$$

$$\left(D_1\nu^2 - \Sigma_1(\omega)\right)\left(D_2\nu^2 - \Sigma_2(\omega)\right) - \nu\Sigma_f(\omega)\Sigma_R = 0 \tag{5.4}$$

chosen so that they are real and positive for $\omega = 0$.

The first term of the Green's function is known as the global component: it is cosine shaped, and varies slowly in comparison with the second one, the local component, which shows up as a peak.

While these results are well known, they have not been employed to calculate the axial noise from propagating perturbations before, nor the noise in the fast group, so the results of such calculations will be presented here to give background to the MSR results.

These calculations have been made using two perturbations: first, one in Σ_{a2} only, and one corresponding to a perturbation in temperature. The temperature was changed by 1°C to see how all of the reactor parameters would be affected. This means that while the perturbations are comparable, they do not necessarily have a typical amplitude. Further, for the BWR, density perturbations (due to void) are much more important, but the temperature perturbation was still used for comparability.

The first thing that should be noted is that for the frequency dependence (Fig. 5.1) of the Green's function, there are distinct "knees" at high frequencies for the G_{22} term: these are due to the local component, which decays more slowly than the global component. Thus, at high enough frequencies, the local component will begin to dominate, and the curve will flatten out.

The second thing is that if we examine the space dependence of the noise from a propagating perturbation (Fig. 5.2), we see the same general behaviour with oscillations, but with one big difference: there is no asymmetry. Thus, this asymmetry seems to be a direct consequence of the moving fuel, not the perturbation.

Third, if we consider the frequency dependence (Fig. 5.3), we see that while there are no deep sinks, there is an oscillating structure: as in one-group

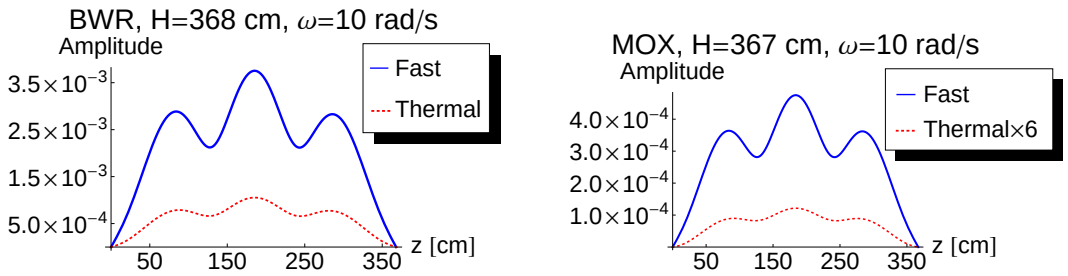

(a) BWR (b) Fast

Figure 5.2: Space dependence of the noise from a propagating perturbation of Σ_{a2}.

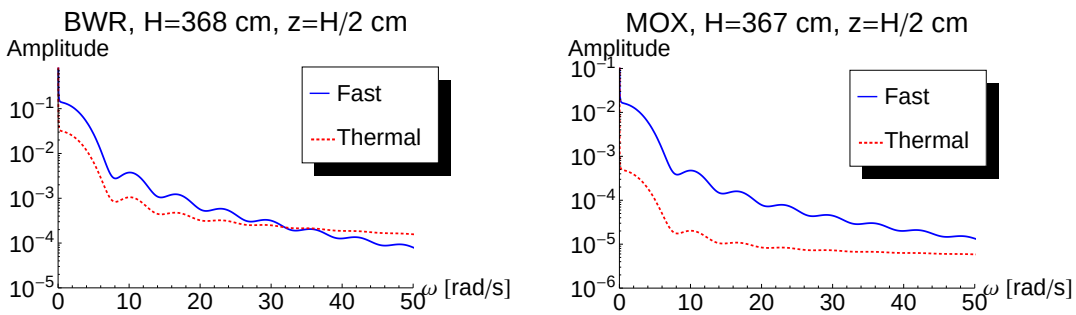

(a) BWR (b) Fast

Figure 5.3: Frequency response to a propagating perturbation in Σ_{a2}.

theory, this is because the reactors are large, and thus, while the point kinetic contribution has a sinusoidal structure, other components are monotonous. When combined, the oscillations become less dominant, or are even masked completely.

Finally, if we briefly consider the noise from a perturbation in temperature, we see that such an approach is necessary for analysis in a real reactor: the noise still has an oscillating spatial structure, but in the case of the fast reactor (Fig. 5.4), there is even a difference in the number of oscillations between the fast and the thermal component. Similarly, the frequency dependence also grow more complex when several cross sections are perturbed at the same time. The details of that are covered in Paper VI.

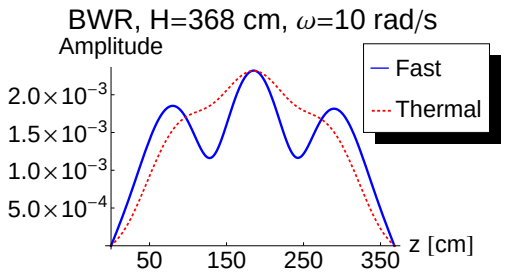

(a) BWR

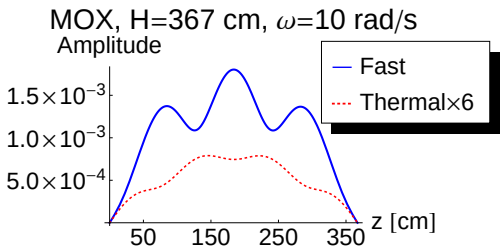

(b) Fast

Figure 5.4: Space dependence of the noise from a propagating temperature perturbation.

5.3 Basic equations for MSRs

The basic equations of the two-group theory are as follows:

$$\frac{1}{v_1}\frac{\partial\phi_1(x,t)}{\partial x} = D_1\nabla^2\phi_1(x,t) + (\nu\Sigma_{f1}(1-\beta) - \Sigma_{a1}(x,t) - \Sigma_R)\,\phi_1(x,t) + \nu\Sigma_{f2}\phi_2(x,t) + \lambda C(x,t) \tag{5.5}$$

$$\frac{1}{v_2}\frac{\partial\phi_2(x,t)}{\partial x} = D_2\nabla^2\phi_2(x,t) + \Sigma_R\phi_1(x,t) - (\Sigma_{f2} + \Sigma_{a2}(x,t))\,\phi_2(x,t) \tag{5.6}$$

$$\frac{\partial C(x,t)}{\partial t} + u\frac{\partial C(x,t)}{\partial x} = \beta\nu\Sigma_{f1}\phi_1(x,t) + \beta\nu\Sigma_{f2}\phi_2(x,t) - \lambda C(x,t) \tag{5.7}$$

Here, we shall neglect fission from fast neutrons, i.e. set $\nu\Sigma_{f1} = 0$. We shall also use the shorthand notation $\Sigma_1 = \Sigma_{a1} + \Sigma_R$. With this, the static equations become, in matrix form

$$\hat{\mathbb{M}}_0(x)\vec{\phi}_0(x) = \begin{pmatrix} D_1\nabla^2 - \Sigma_1 & \nu\Sigma_f(1-\beta) & \lambda \\ \Sigma_R & D_2\nabla^2 - \Sigma_{a2} & 0 \\ 0 & \beta\nu\Sigma_f & -u\frac{\partial}{\partial x} - \lambda \end{pmatrix} \begin{bmatrix} \phi_1(x) \\ \phi_2(x) \\ C_0(x) \end{bmatrix} = 0, \tag{5.8}$$

with boundary conditions

$$\phi_i(\pm a) = 0, \quad C_0(-a) = C_0(a)e^{-\lambda\tau_L}. \tag{5.9}$$

Using the same technique as in one-group theory to eliminate the equation for the delayed neutron precursors, it can be rewritten as

$$D_1\nabla^2\phi_1(x) - \Sigma_1\phi_1(x) + \nu\Sigma_f(1-\beta)\phi_2(x) + e^{-\frac{x\lambda}{u}}\frac{\lambda\beta\nu\Sigma_f}{u}\left(\frac{1}{e^{\lambda\tau}-1}\int_{-a}^{a} e^{\frac{\lambda x'}{u}}\phi_2(x')dx' + \int_{-a}^{x} e^{\frac{\lambda x'}{u}}\phi_2(x')dx'\right) = 0 \tag{5.10}$$

$$D_2\nabla^2\phi_2(x) - \Sigma_{a2}\phi_2(x) + \Sigma_R\phi_1(x) = 0. \tag{5.11}$$

Again, this is not a self-adjoint set of equations, and such a set will have to be constructed in order to obtain the adjoint flux. This is done in exactly the same manner as in the one-group theory, giving

$$\hat{\mathbb{M}}_0^\dagger(x) = \begin{pmatrix} D_1\nabla^2 - \Sigma_1 & \Sigma_R & 0 \\ \nu\Sigma_f(1-\beta) & D_2\nabla^2 - \Sigma_2 & \beta\nu\Sigma_f \\ \lambda & 0 & u\frac{\partial}{\partial x} - \lambda \end{pmatrix}. \tag{5.12}$$

with boundary conditions

$$\phi_i^\dagger(\pm a) = 0 \quad C_0^\dagger(-a) = C_0^\dagger(a)e^{\lambda\tau_L}. \tag{5.13}$$

The proof of this being the adjoint follows from that for one-group theory.

Equations for the noise will also follow the pattern from one-group theory, with λ replaced by $\lambda + i\omega$ almost everywhere, and Σ_i by $\Sigma_j(\omega) = \Sigma_j + i\omega/v_j$:

$$\begin{aligned} &D_1\nabla^2\delta\phi_1(x,\omega) - \Sigma_1(\omega)\delta\phi_1(x,\omega) + \nu\Sigma_f(1-\beta)\delta\phi_2(x,\omega) \\ &\quad + e^{-\frac{x(\lambda+i\omega)}{u}}\frac{\lambda\beta\nu\Sigma_f}{u}\left(\frac{1}{e^{(\lambda+i\omega)\tau}-1}\int_{-a}^{a} e^{\frac{(\lambda+i\omega)x'}{u}}\delta\phi_2(x',\omega)dx'\right. \\ &\quad \left. + \int_{-a}^{x} e^{\frac{(\lambda+i\omega)x'}{u}}\delta\phi_2(x',\omega)dx'\right) = S_1(x,\omega) \end{aligned} \tag{5.14}$$

$$D_2\nabla^2\delta\phi_2(x,\omega) - \Sigma_{a2}(\omega)\delta\phi_2(x,\omega) + \Sigma_R\delta\phi_1(x,\omega) = S_2(x,\omega). \tag{5.15}$$

5.4 Infinite fuel velocity

As for the one-group theory, we start with investigating the case of infinite fuel velocity. The static equations are

$$D_1\nabla^2\phi_1(x) - \Sigma_1\phi_1(x) + \nu\Sigma_f(1-\beta)\phi_2(x) + \frac{\beta\nu\Sigma_f}{T}\int_{-a}^{a}\phi_2(x')dx' = 0 \tag{5.16}$$

$$D_2\nabla^2\phi_2(x) - \Sigma_{a2}\phi_2(x) + \Sigma_R\phi_1(x) = 0. \tag{5.17}$$

with solutions

$$\vec{\phi}_0(x) = A\begin{bmatrix} 1 \\ c_\mu \end{bmatrix}(\cos(\mu x) - \cos(\mu a)) + B\begin{bmatrix} 1 \\ c_\nu \end{bmatrix}(\cosh(\nu x) - \cosh(\nu a)), \tag{5.18}$$

where

$$c_\mu = \frac{\Sigma_R}{\Sigma_{a2} + D_2\mu^2} \text{ and } c_\nu = \frac{\Sigma_R}{\Sigma_{a2} - D_2\nu^2}. \tag{5.19}$$

Here μ and ν are the positive roots of

$$\mu^2 = -\frac{1}{2}\left(\frac{\Sigma_1}{D_1} + \frac{\Sigma_{a2}}{D_2}\right) + \frac{1}{2}\sqrt{\left(\frac{\Sigma_1}{D_1} + \frac{\Sigma_{a2}}{D_2}\right)^2 - \frac{4}{D_1D_2}\left(\Sigma_1\Sigma_{a2} - \Sigma_R\nu\Sigma_f(1-\beta)\right)} \tag{5.20}$$

$$\nu^2 = \frac{1}{2}\left(\frac{\Sigma_1}{D_1} + \frac{\Sigma_{a2}}{D_2}\right) + \frac{1}{2}\sqrt{\left(\frac{\Sigma_1}{D_1} + \frac{\Sigma_{a2}}{D_2}\right)^2 - \frac{4}{D_1D_2}\left(\Sigma_1\Sigma_{a2} - \Sigma_R\nu\Sigma_f(1-\beta)\right)}. \tag{5.21}$$

Table 5.2: Estimated thermal to fast spectral ratios for the three systems considered

	Thorium	BWR	Fast reactor
Σ_R/Σ_{a2}	1.14	0.25	0.030

The constant B can be found to be related to A as

$$B = \frac{\mu^2 c_\mu \cos(\mu a)}{\nu^2 c_\nu \cosh(\nu a)} A \tag{5.22}$$

while A is left as a free parameter as the equations are homogeneous. We still need a criticality equation though, which we get if we insert the solution in the system and require A to be non-zero, which yields the following transcendental equation.

$$\begin{aligned}
&\cos(\mu a)\left(-\nu\Sigma_f(1-\beta)c_\mu\left(1-\frac{\mu^2}{\nu^2}\right)+\Sigma_1\left(1-\frac{\mu^2}{\nu^2}\frac{c_\mu}{c_\nu}\right)\right)\\
&+\frac{\beta\nu\Sigma_f}{T}c_\mu\Bigg(\left(\frac{2}{\mu}\sin(\mu a)-2a\cos(\mu a)\right)\\
&-\left(\frac{2}{\nu}\sinh(\nu a)-2a\cosh(\nu a)\right)\frac{\mu^2}{\nu^2}\frac{\cos(\mu a)}{\cosh(\nu a)}\Bigg)=0.
\end{aligned} \tag{5.23}$$

Again, this can not be given a simple closed-form solution, and has to be solved numerically.

The static fluxes of the three systems are shown in Fig. 5.5. As in one-group theory, these are not very different from the results in traditional reactors, since the symmetry of the core is restored at infinite velocity.

The ratio between the fast and thermal fluxes differs largely between the systems: the thorium reactor has the softest spectrum, with larger thermal than fast flux, the fast reactor has – as expected – a very hard spectrum, and the BWR is somewhere in between. By neglecting leakage, it is easy to get an approximation of the ratio between the fluxes as

$$\frac{\phi_2(x)}{\phi_1(x)} \approx \frac{\Sigma_R}{\Sigma_{a2}}. \tag{5.24}$$

The values of this expression are given in Table 5.2, and as can be seen when comparing with Fig. 5.5, it predicts the behaviour well.

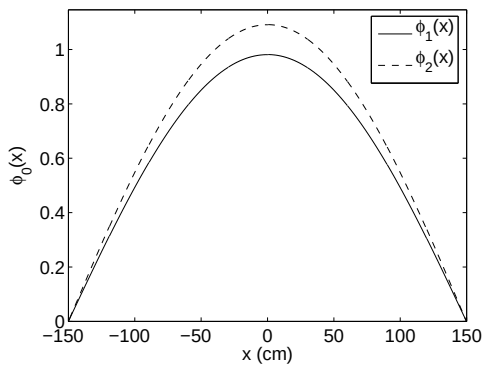

(a) Thorium

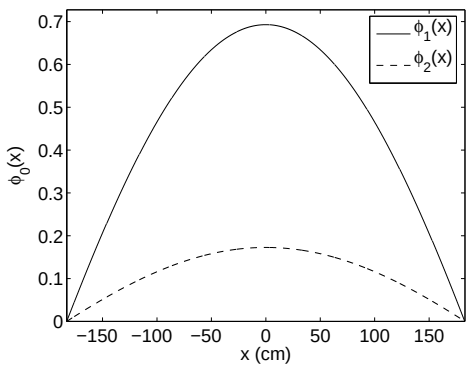

(b) BWR

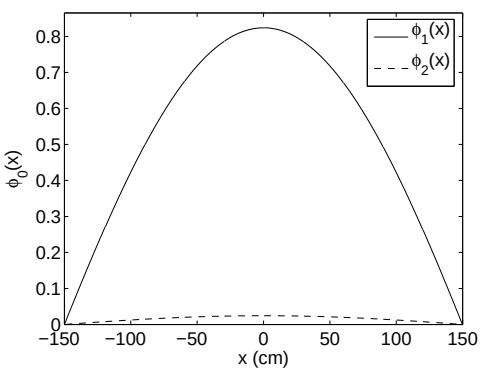

(c) Fast reactor

Figure 5.5: Static fluxes in the three systems considered for infinite fuel velocity

5.4.1 Dynamic behaviour

The noise equations are

$$D_1\nabla^2\delta\phi_1(x,\omega) - \Sigma_1(\omega)\delta\phi_1(x,\omega) + \nu\Sigma_f(1-\beta)\delta\phi_2(x,\omega) + \frac{\beta\nu\Sigma_f}{T}\frac{\lambda}{\lambda+i\omega}\int_{-a}^{a}\delta\phi_2(x',\omega)dx' = S_1(x,\omega) \tag{5.25}$$

$$D_2\nabla^2\delta\phi_2(x,\omega) - \Sigma_2(\omega)\delta\phi_2(x,\omega) + \Sigma_R\delta\phi_1(x,\omega) = S_2(x,\omega). \tag{5.26}$$

We shall solve them using Green's functions. Normally, when using two or more groups, the adjoint equations are preferred, at least if one is only concerned with detection in the thermal spectrum. However, as many Generation IV systems, including some MSR designs, operate with fast spectrums, and hence the fast flux and the fast noise is also of interest, that advantage disappears, and it does not, in theory, matter which set of Green's functions is used, even if numerical considerations might give one an advantage over the other.

If we write the equations in matrix form, we have

$$\hat{\mathbb{M}}(\omega)\hat{G}(x,x_p,\omega) = \hat{I}\delta(x-x_p) \tag{5.27}$$

where

$$\hat{\mathbb{M}}(\omega) = \begin{pmatrix} D_1\nabla^2 - \Sigma_1(\omega) & \nu\Sigma_f(1-\beta) + \frac{\eta(\omega)}{T}\int_{-a}^{a}dx \\ \Sigma_R & D_2\nabla^2 - \Sigma_2(\omega) \end{pmatrix}, \tag{5.28}$$

$$\hat{G}(x,x_p,\omega) = \begin{pmatrix} G_{11}(x,x_p,\omega) & G_{12}(x,x_p,\omega) \\ G_{21}(x,x_p,\omega) & G_{22}(x,x_p,\omega) \end{pmatrix}, \tag{5.29}$$

and $\hat{I}$ is the 2×2 unit matrix.

G_{11} is the noise in the fast group from a fast source, G_{12} is the noise in the fast group from a thermal source, G_{21} is the noise in the thermal group from a fast source, and G_{22} is the noise in the thermal group from a thermal source.

Again using the trick of dividing the matrix into two parts, we let

$$\hat{G}(x,x_p,\omega) = \hat{G}_i(x,x_p,\omega) + \hat{G}_h(x,x_p,\omega) \tag{5.30}$$

where the two parts are chosen so that

$$\hat{\mathbb{M}}'(\omega)\hat{G}_i(x,x_p,\omega) = \hat{I}\delta(x-x_p) \tag{5.31}$$

and

$$\hat{\mathbb{M}}(\omega)\hat{G}_h(x,x_p,\omega) = -\left(\hat{\mathbb{M}}(\omega) - \hat{\mathbb{M}}'(\omega)\right)\hat{G}_i(x,x_p,\omega) \tag{5.32}$$

where

$$\hat{\mathbb{M}}'(\omega) = \begin{pmatrix} D_1\nabla^2 - \Sigma_1(\omega) & \nu\Sigma_f(1-\beta) \\ \Sigma_R & D_2\nabla^2 - \Sigma_2(\omega) \end{pmatrix}. \tag{5.33}$$

It is again relatively easy to solve for $\hat{G}_i$; the solution will be similar to what was obtained for traditional reactors. If we define

$$G_i(x,x_p,\omega) = \frac{1}{D_1 D_2(\nu^2+\mu^2)} \begin{cases} \frac{\sin\mu(a-x_p)\sin\mu(a+x)}{\mu\sin 2\mu a} - \frac{\sinh\nu(a-x_p)\sinh\nu(a+x)}{\nu\sinh 2\nu a} & x < x_p \\ \frac{\sin\mu(a+x_p)\sin\mu(a-x)}{\mu\sin 2\mu a} - \frac{\sinh\nu(a+x_p)\sinh\nu(a-x)}{\nu\sinh 2\nu a} & x > x_p \end{cases}, \tag{5.34}$$

we will have

$$G_i^{11}(x,x_p,\omega) = \left(D_2\nabla^2 - \Sigma_2(\omega)\right) G_i(x,x_p,\omega) \tag{5.35}$$
$$G_i^{12}(x,x_p,\omega) = -\nu\Sigma_f(1-\beta)G_i(x,x_p,\omega) \tag{5.36}$$
$$G_i^{21}(x,x_p,\omega) = -\Sigma_R G_i(x,x_p,\omega) \tag{5.37}$$
$$G_i^{22}(x,x_p,\omega) = \left(D_1\nabla^2 - \Sigma_1(\omega)\right) G_i(x,x_p,\omega). \tag{5.38}$$

The parameters $\mu = \mu(\omega)$ and $\nu = \nu(\omega)$ are then the roots of

$$\left(D_1\mu^2 + \Sigma_1(\omega)\right)\left(D_2\mu^2 + \Sigma_2(\omega)\right) - \nu\Sigma_f(1-\beta)\Sigma_R = 0 \tag{5.39}$$
$$\left(D_1\nu^2 - \Sigma_1(\omega)\right)\left(D_2\nu^2 - \Sigma_2(\omega)\right) - \nu\Sigma_f(1-\beta)\Sigma_R = 0 \tag{5.40}$$

chosen so that they are real and positive for $\omega = 0$.

The remainder term, $\hat{G}_h$ will have the same general form as the static flux, i.e.

$$\begin{bmatrix} G_h^{1j}(x,x_p,\omega) \\ G_h^{2j}(x,x_p,\omega) \end{bmatrix} = A^j \begin{bmatrix} 1 \\ c_\mu \end{bmatrix} (\cos(\mu x) - \cos(\mu a)) + B^j \begin{bmatrix} 1 \\ c_\nu \end{bmatrix} (\cosh(\nu x) - \cosh(\nu a)). \tag{5.41}$$

where

$$c_\mu = c_\mu(\omega) = \frac{\Sigma_R}{\Sigma_2(\omega) + D_2\mu^2} \text{ and } c_\nu = c_\nu(\omega) = \frac{\Sigma_R}{\Sigma_2(\omega) - D_2\nu^2}. \tag{5.42}$$

A^j and B^j will be determined similarly to how they were in one-group theory.

The frequency dependence of the magnitude of the four components of the Green's function for all three reactors is shown in Fig. 5.6. Two things can be seen: that the different components have very similar behaviour up to very high frequencies, a behaviour that is similar to the zero power transfer function and that we have already encountered in the one-group theory. The lower break frequency is also rather similar between the reactors, since it depends on the delayed neutron decay constant λ which is similar for all three reactors. The upper break frequency (the end of the plateau region), instead is roughly at β/Λ, where Λ is the prompt neutron generation time. The generation time is

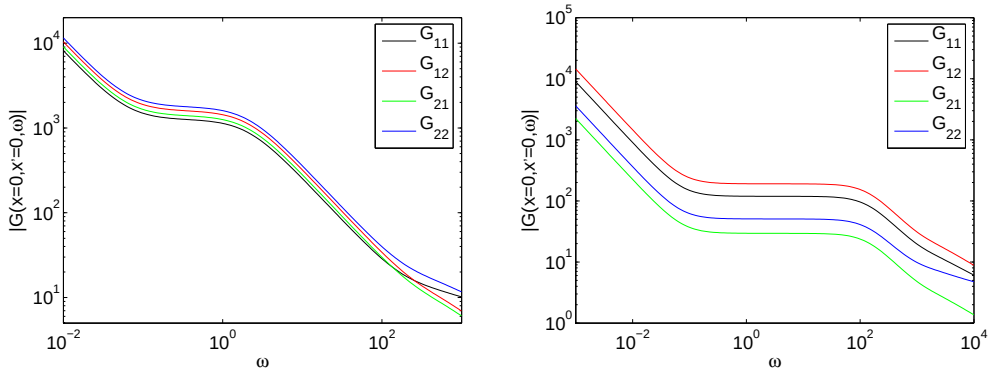

(a) Thorium

(b) BWR

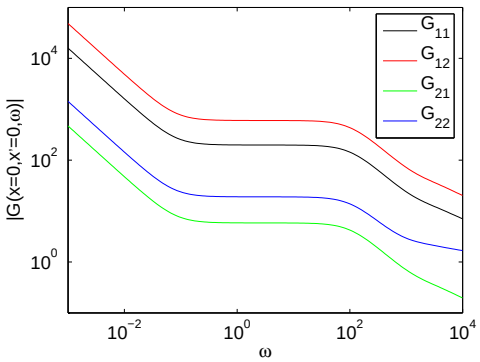

(c) Fast reactor

Figure 5.6: Frequency dependence of the Green's functions, infinite velocity. $x = 0$, $x_p = 0$.

much longer in the thorium reactor, as it uses graphite as a moderator, which leads to a much shorter plateau region. The fraction of delayed neutrons β also varies between the reactors, but not with orders of magnitude as Λ. We can also see the breaks where the local component starts to dominate.

The different components also have differing amplitudes, similar to the static fluxes. The differences in the Green's functions can be at least partially predicted from these: for the Thorium reactor the Green's functions have similar amplitudes, just as the static fluxes had. The differences are larger in the BWR-analogue, and largest in the fast reactor.

From here on, we shall use the dynamic adjoint. If we consider a point-

detector of thermal neutrons placed in x_0, the adjoints Ψ are obtained from

$$\hat{\mathbb{M}}^{\dagger}\vec{\Psi}(x,x_p,\omega) = \begin{pmatrix} D_1\nabla^2 - \Sigma_1(\omega) & \Sigma_R \\ \nu\Sigma_f(1-\beta) + \frac{\beta\nu\Sigma_f}{T}\frac{\lambda}{\lambda+i\omega}\int_{-a}^{a} dx & D_2\nabla^2 - \Sigma_2(\omega) \end{pmatrix} \times \\ \times \begin{bmatrix} \Psi_1(x,x_p,\omega) \\ \Psi_2(x,x_p,\omega) \end{bmatrix} = \begin{bmatrix} 0 \\ \delta(x-x_p) \end{bmatrix} \tag{5.43}$$

The space dependence of the adjoints is shown for all three systems in Figs. 5.7–5.9 for a detector placed in the middle of a reactor at $x_0 = 0$, at two different frequencies: $\omega = 10$ and $\omega = 1000$ rad/s. The lower frequency lies well within the region of a MSR where point-kinetic theory would be applicable in a one-group treatment[a], and while the higher frequency is unrealistic to use in actual measurements, it is also firmly in the area where point-kinetics breaks down. The need for such high frequencies is the main result from the one-group theory: a MSR behaves more point-kinetic than a corresponding traditional reactors of the same size, which means that space-dependent components appear at higher frequencies. It has to be noted also that 1000 rad/s is actually much more than what is needed for the thorium reactor, but it was chosen to facilitate comparison.

At the lower frequency, all three reactors show point-kinetic behaviour, but especially the thorium reactor. Here, not only the circulating fuel but also the smaller fraction of delayed neutrons contribute to the point-kinetic dominance, by causing the neutron chains to be longer than in the other reactor types, which gives a stronger spatial coupling. Thus, the local component that normally can be distinguished in the thermal adjoint Ψ_2 is not visible for the thorium reactor, but in neither the BWR-analogue or the fast reactor is it very pronounced. We will return to this behaviour later, in the finite-velocity treatment.

At the higher frequency, where the local component has gained in importance relative to the global component, it is clearly visible in the BWR-analogue and the fast reactor. In the thorium reactor, it is still hard to clearly distinguish, paradoxically because it is too dominant, and is less localiseddue to a longer diffusion length, while the global (point kinetic plus space dependent) component has become more localised. One can by looking at lower frequencies see that the relaxation length of the local component is roughly equal to the region were the two adjoints have a large difference in magnitude (plot not given here for brevity).

5.4.2 Propagating perturbation

Similar to the case of one-group theory, we will now consider the noise induced by a perturbation propagating through the reactor at a finite velocity u_p.

In a BWR, where such perturbations usually are considered, they would be in the moderator, and are thus usually modelled as pertaining to the removal

[a] A traditional reactor would already be space-dependent.

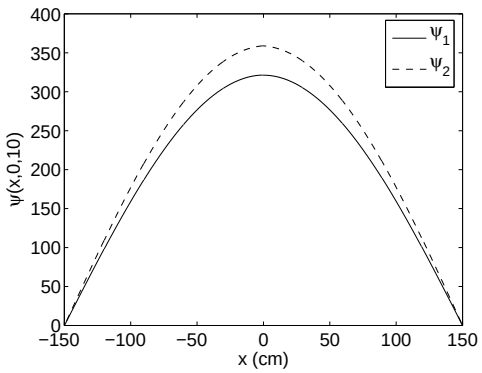

(a) $\omega = 10$ rad/s

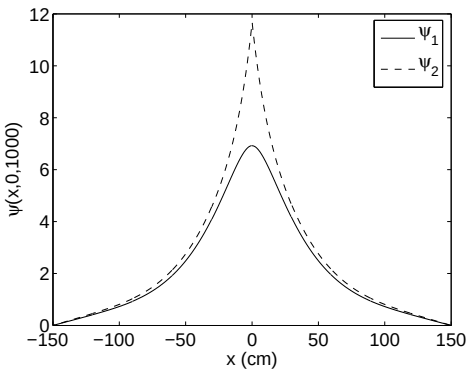

(b) $\omega = 1000$ rad/s

Figure 5.7: Adjoint Green's functions, infinite velocity. $x_0 = 0$. Thorium.

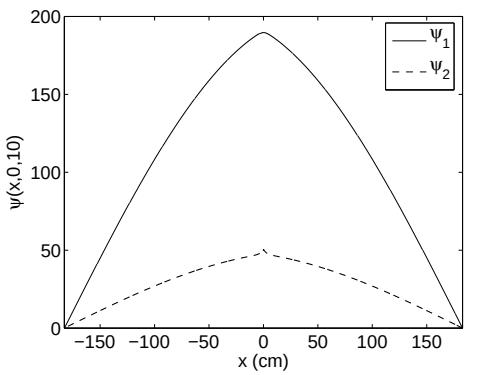

(a) $\omega = 10$ rad/s

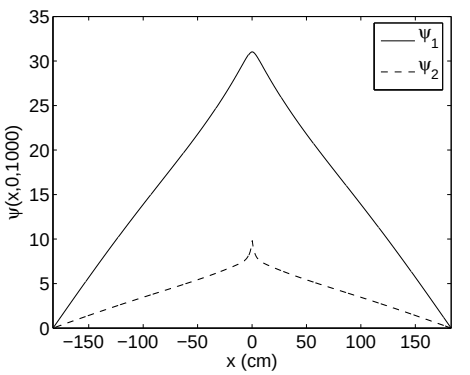

(b) $\omega = 1000$ rad/s

Figure 5.8: Adjoint Green's functions, infinite velocity. $x_0 = 0$. BWR.

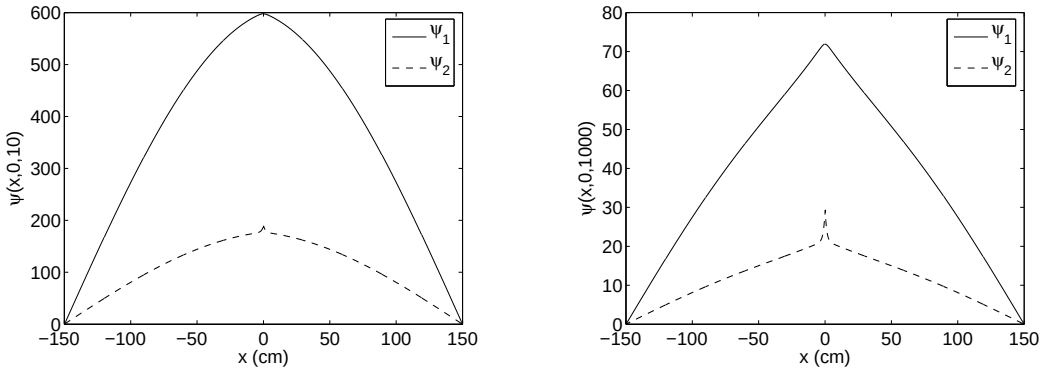

(a) $\omega = 10$ rad/s

(b) $\omega = 1000$ rad/s

Figure 5.9: Adjoint Green's functions, infinite velocity. $x_0 = 0$. Fast reactor. Ψ_2 has been multiplied with a factor 10 for visibility.

cross section. In a MSR, however, the moderator is stationary, and it is the fuel that moves. Furthermore, there is no boiling, so such perturbations would be from density and temperature variations, fission product distributions etc. and it is reasonable to model the perturbations as fluctuations in the thermal absorption cross section Σ_{a2}. The fact that they are propagating is then expressed as

$$\delta\Sigma_{a2}(x,\omega) = e^{\frac{-i\omega(x+a)}{u_p}}\delta\Sigma_{a2}(-a,\omega) \tag{5.44}$$

and the noise is given by

$$\delta\vec{\phi}(x,\omega) = \int_{-a}^{a} \hat{G}(x,x_p,\omega)\vec{S}(x_p,\omega)dx_p \tag{5.45}$$

where

$$\vec{S}(x,\omega) = \begin{bmatrix} 0 \\ \phi_2(x)\delta\Sigma_{a2}(x,\omega), \end{bmatrix}, \tag{5.46}$$

The frequency dependence of the noise induced by a propagating perturbation is shown in Fig. 5.10. The sink structure we saw in the one-group theory and in some of the stationary-fuel reactors is still there: more pronounced in the fast noise, but visible in both (at least at low frequencies).

The space dependence of the noise, for four different frequencies, is shown in Figs. 5.11–5.13. The spatial oscillations that can be seen will not be discussed here, as it was already done in the one-group section and no new features have appeared. One thing that can be noted, however, is that the larger oscillations in the frequency dependence are reflected in the space dependence; it is perhaps easiest to see in Fig. 5.12, where the valleys have roughly the same magnitude for both fast and thermal noise, but where the peaks are much higher for the fast noise, just as the oscillations of the fast noise are more pronounced in Fig. 5.10(b).

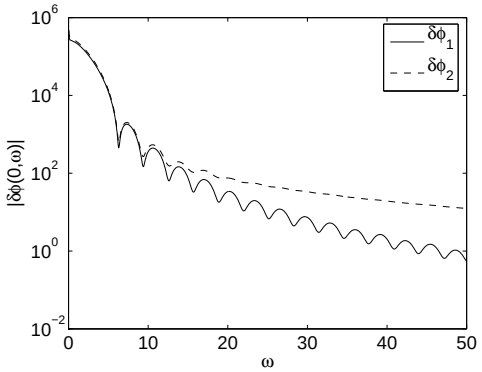

(a) Thorium

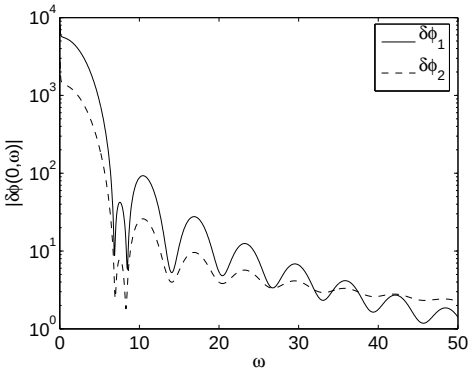

(b) BWR

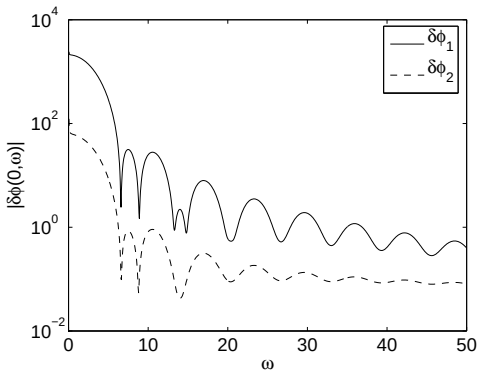

(c) Fast reactor

Figure 5.10: Frequency dependence of noise, perturbation velocity $u_p = H/2$ s^{-1}, infinite fuel velocity

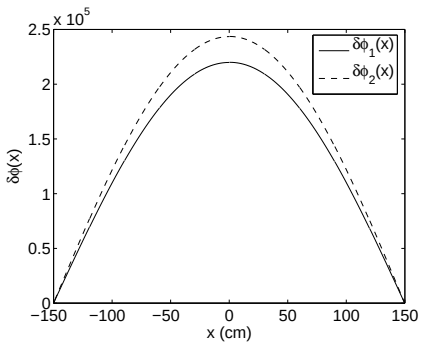

(a) $\omega = 1$ rad/s

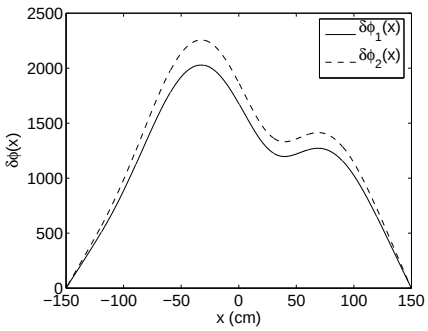

(b) $\omega = 7$ rad/s

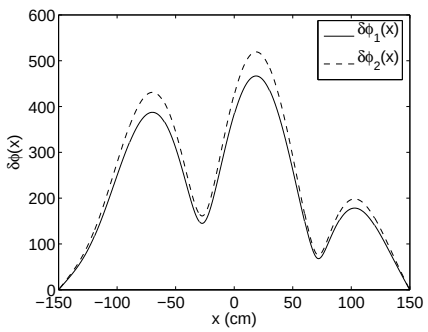

(c) $\omega = 10$ rad/s

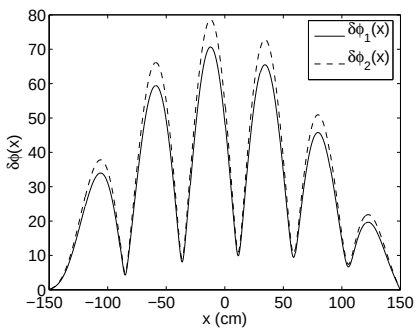

(d) $\omega = 20$ rad/s

Figure 5.11: Noise, perturbation velocity $u_p = H/2\ s^{-1}$, infinite fuel velocity. $x_p = 0$. Thorium fuel.

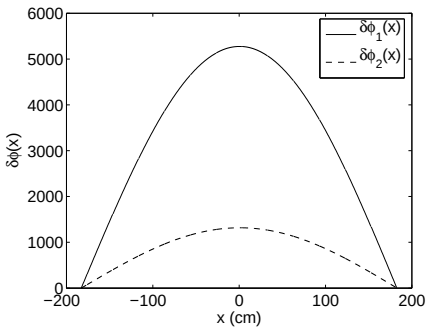

(a) $\omega = 1$ rad/s

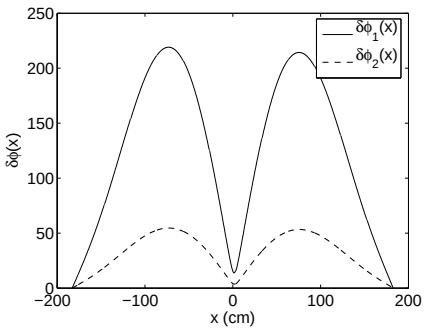

(b) $\omega = 7$ rad/s

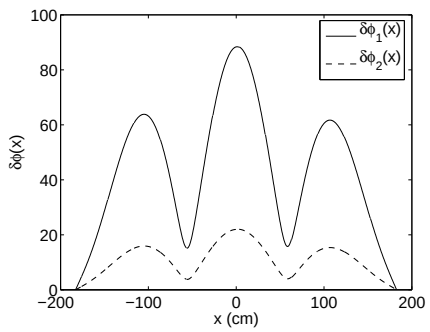

(c) $\omega = 10$ rad/s

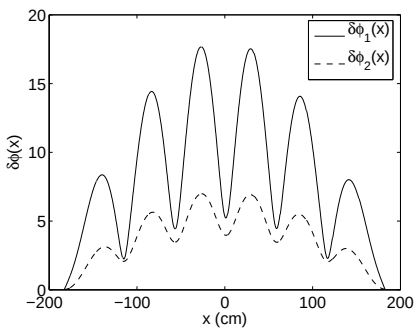

(d) $\omega = 20$ rad/s

Figure 5.12: Noise, perturbation velocity $u_p = H/2\ s^{-1}$, infinite fuel velocity. $x_p = 0$. BWR.

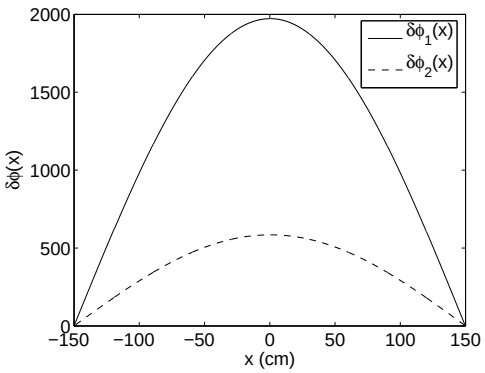

(a) $\omega = 1$ rad/s

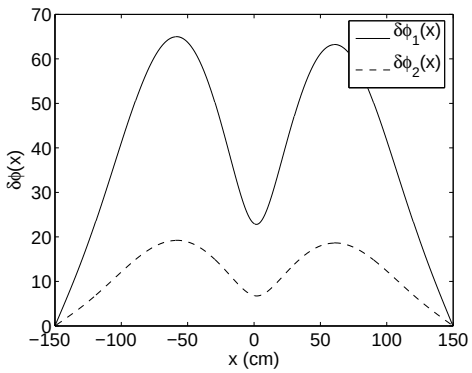

(b) $\omega = 7$ rad/s

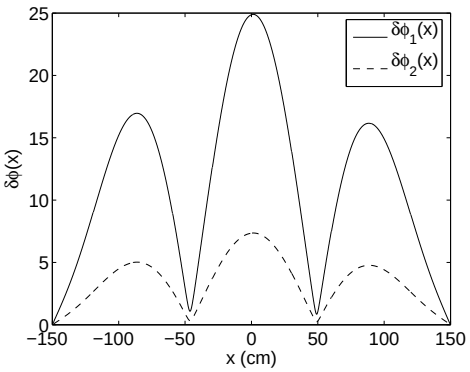

(c) $\omega = 10$ rad/s

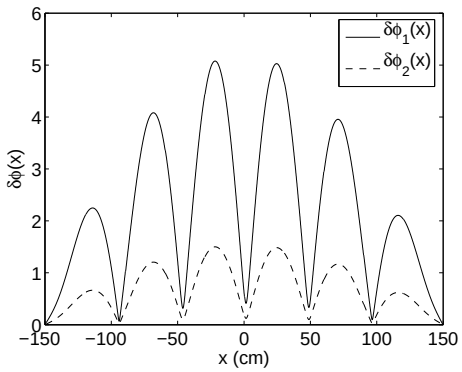

(d) $\omega = 20$ rad/s

Figure 5.13: Noise, perturbation velocity $u_p = H/2\ s^{-1}$, infinite fuel velocity. $x_p = 0$. Fast reactor. $\delta\Phi_2$ has been multiplied by a factor 10 for visibility.

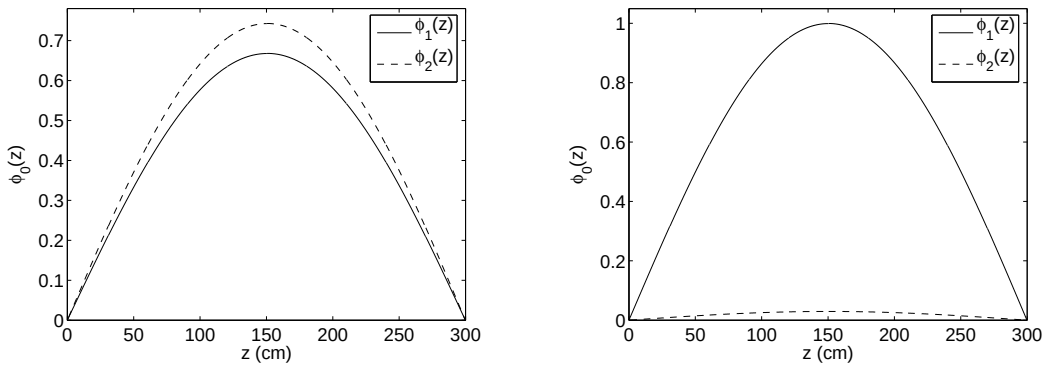

(a) Thorium

(b) Fast reactor

Figure 5.14: Static flux. $u = 20$ cm/s.

5.5 Finite velocity

Also for finite velocities, there are large similarities between one- and two-group theory: however, the equations have not been solved exactly, rather, the static flux has been approximated by a truncated Fourier series while the (adjoint) Green's functions were divided into two parts: G_h, solved analytically, and G_i, approximated by another truncated Fourier series. We thus have

$$\phi_i(z) = \sum_{n=1}^{N} a_{i,n} \sin B_n z \tag{5.47}$$

and

$$G_i^{ij}(z, z', \omega) = \sum_{n=1}^{N} \bar{a}_{ij,n}(z', \omega) \sin B_n z, \tag{5.48}$$

where $B_n = n\pi/H$ and $i, j = 1, 2$ are the energy group index, here as superscripts for the Green's function. The coordinates were changed to $z = x + a$ for practical purposes.

5.5.1 Static flux

The static fluxes are similar to those of infinite velocity (Fig. 5.14); unlike the one-group result, the asymmetry is not so large as to be easily distinguishable by the eye, and therefore vary less with fuel velocity. This is mostly because the diffusion length L_D is much shorter in the system used in the one-group treatment, so while the differences in neutron precursor distribution are not very large between systems (compare Figs. 4.2 and 5.15), the redistribution has a much bigger impact in the one-group system.

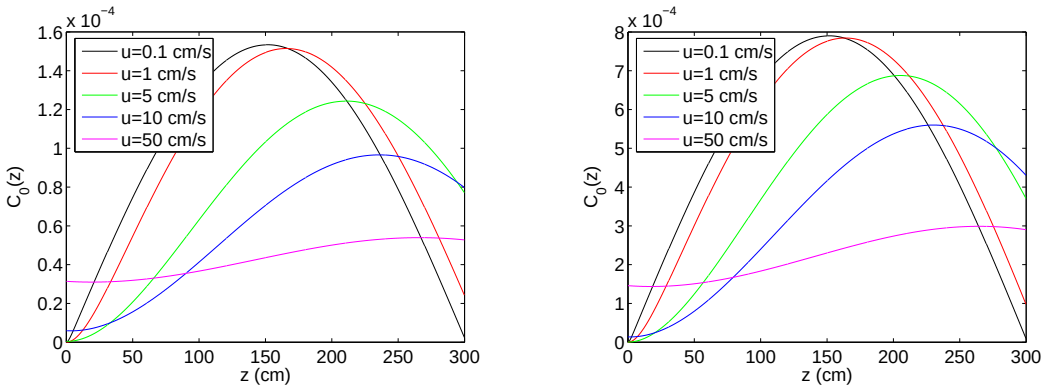

(a) Thorium

(b) Fast reactor

Figure 5.15: Delayed neutron precursor distribution.

5.5.2 Adjoint Green's functions

The adjoint Green's functions will, as mentioned earlier, be constructed out of two parts, called "inhomogeneous" and "homogeneous" (despite both being determined by inhomogeneous equations). The first of these is similar to the full Green's function of a traditional reactor, and the latter is a numerical expansion of the rest terms, i.e. the ones coming from the redistribution of the delayed neutron precursors through the fuel flow. The first of these terms offers no new challenges, but it is necessary to make a short remark about the numerics of the second part.

First, it should be noted, that while in the one-group theory the total number of terms in the expansion was limited due to the need to solve a matrix equation to obtain the final solution, the fact that we now need twice as many terms to get the same level of accuracy is not a serious impediment: the matrix in question is actually quite sparse (it can be constructed out of four quadratic sub-matrices, and three of these only have diagonal elements), so numerical accuracy is not seriously affected.

Second, there is now a difference between the normal and the adjoint Green's functions in the numerics: the normal equations have problems with handling the BWR-analogue, while the adjoint equations diverge at very low velocities (the limit seems to be at slightly less than 1 cm/s), due to some rearrangements of the delayed neutron precursor terms. In practice, this has very little effect, as the velocity in a real MSR would most likely be much higher, and the difference when compared with a traditional reactor is not very great at so low velocities. This would of course also have been avoided by using the analytical solution.

The results for the dynamic adjoint function resemble to a large extent to the results obtained for the case of infinite velocity, and the deviations follow the same pattern that was seen in the one-group calculations: the amplitudes at different frequencies change in a similar manner, and the extra peaks that

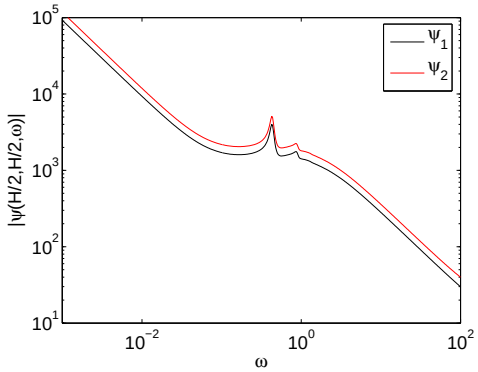

(a) Ψ_1 & Ψ_2. $u = 50$ cm/s

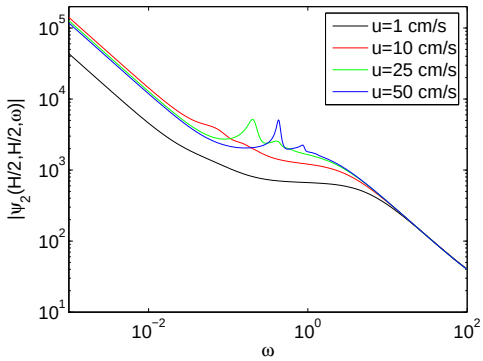

(b) Velocity dependence of Ψ_2

Figure 5.16: Adjoint Green's functions, finite velocity. $z = H/2$, $z' = H/2$. Thorium.

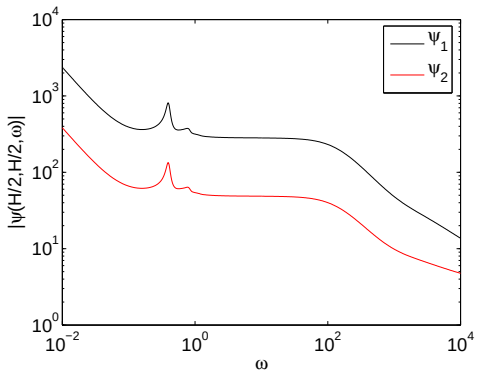

(a) Ψ_1 & Ψ_2. $u = 50$ cm/s

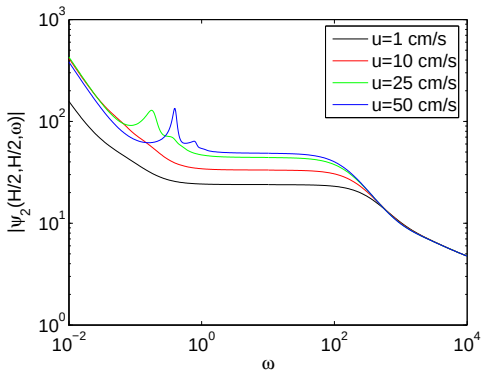

(b) Velocity dependence of Ψ_2

Figure 5.17: Adjoint Green's functions, finite velocity. $z = H/2$, $z' = H/2$. BWR.

show up have the same velocity dependence as in one-group theory, while the different components have similar ratios of magnitude as in the infinite fuel velocity case (Figs. 5.16–5.18).

The space dependence (Figs. 5.19–5.21) also follows a pattern that could be expected: as in the one-group theory, higher velocities lead to more point-kinetic behaviour. We can, however, note that this effect is strongest in the fast reactor, and weakest in the thorium reactor. Moreover, the relative smallness of the local component in MSRs is not due to it having a smaller amplitude, but rather that the global component is larger, which makes the local component have a smaller relative height.

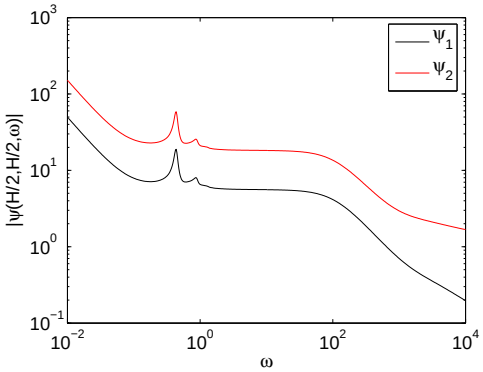

(a) Ψ_1 & Ψ_2. $u = 50$ cm/s

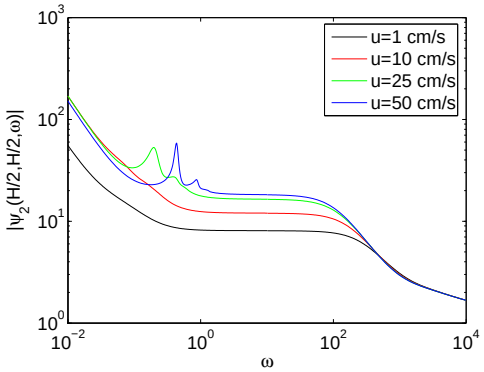

(b) Velocity dependence of Ψ_2

Figure 5.18: Adjoint Green's functions, finite velocity. $z = H/2$, $z' = H/2$. Fast reactor.

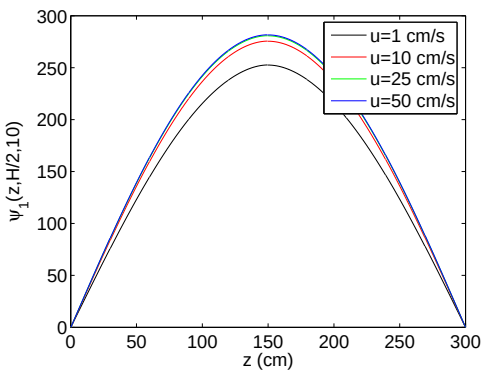

(a) Ψ_1

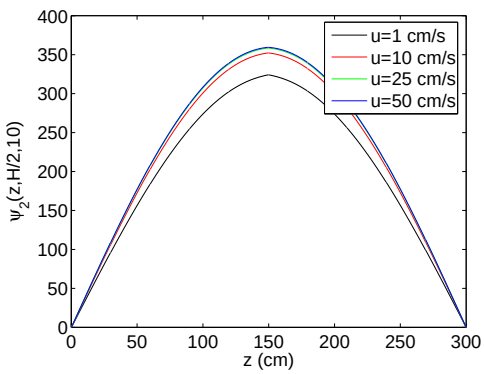

(b) Ψ_2

Figure 5.19: Adjoint Green's functions, velocity dependence. $z' = H/2$, $\omega = 10$ rad/s. Thorium.

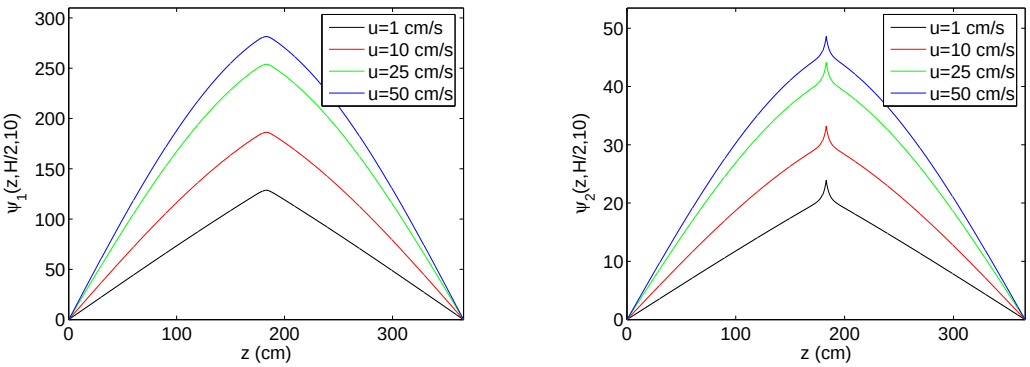

(a) Ψ_1 (b) Ψ_2

Figure 5.20: Adjoint Green's functions, velocity dependence. $z' = H/2$, $\omega = 10$ rad/s. BWR.

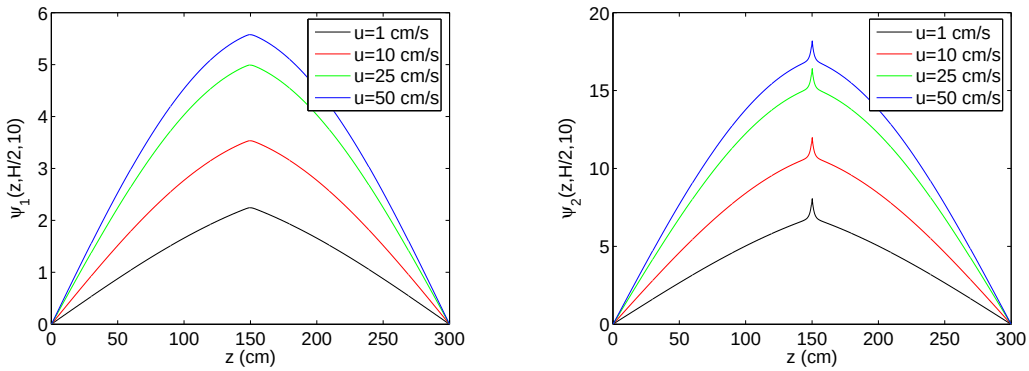

(a) Ψ_1 (b) Ψ_2

Figure 5.21: Adjoint Green's functions, velocity dependence. $z' = H/2$, $\omega = 10$ rad/s. Fast reactor.

CHAPTER 6

MULTI-REGION THEORY

Den dygdigaste man är den som bäst räknar, och de grövsta brott härröra nödvändigt av något fel i Subtraktionen
—Johan Henrik Kellgren, *Patriotisk blick åt Litteraturen*

This chapter covers analytical solutions for multi-region systems. Instead of the usual approach using the adjoint functions, the forward Green's function and the fast noise are calculated. This was originally motiveted by a wish to do a multi-region calculation for the MSR to better encode the differing boundary condition.

6.1 Equations

The basic static two-group equations and their solutions for a three-region, symmetric reactor, with core edges at $x = \pm a$ and where the flux are set to zero at $x = \pm(a+b)$, are well known. They, and the corresponding equations for the Green's functions, are given in Paper V (note the differences in notation). Here, we will give the general solutions for the Green's functions:

$$\vec{G}_1^j = A_1 \begin{bmatrix} 1 \\ c_r \end{bmatrix} \sinh \kappa_1(b+x) + A_2 \begin{bmatrix} 0 \\ 1 \end{bmatrix} \sinh \kappa_2(b+x) \tag{6.1}$$

$$\vec{G}_2^j = A_3 \begin{bmatrix} 1 \\ c_\mu \end{bmatrix} \cos \mu x + A_4 \begin{bmatrix} 0 \\ c_\mu \end{bmatrix} \sin \mu x + A_5 \begin{bmatrix} 1 \\ c_\lambda \end{bmatrix} e^{\lambda x} + A_6 \begin{bmatrix} 0 \\ c_\lambda \end{bmatrix} e^{-\lambda x} \tag{6.2}$$

$$\vec{G}_3^j = A_7 \begin{bmatrix} 1 \\ c_\mu \end{bmatrix} \cos \mu x + A_8 \begin{bmatrix} 0 \\ c_\mu \end{bmatrix} \sin \mu x + A_9 \begin{bmatrix} 1 \\ c_\nu \end{bmatrix} e^{\nu x} + A_{10} \begin{bmatrix} 0 \\ c_\nu \end{bmatrix} e^{-\nu x} \tag{6.3}$$

$$\vec{G}_4^j = A_{11} \begin{bmatrix} 1 \\ c_r \end{bmatrix} \sinh \kappa_1(b-x) + A_{12} \begin{bmatrix} 0 \\ 1 \end{bmatrix} \sinh \kappa_2(b-x) \tag{6.4}$$

where

$$\vec{G}_i^j = \begin{bmatrix} G_i^{1j}(x, x', \omega) \\ G_i^{2j}(x, x', \omega) \end{bmatrix}; \quad j = 1, 2 \tag{6.5}$$

and where the notation that shows the dependence of c, κ, λ and ν on ω have been dropped.

Now, the interface conditions (at the core boundaries $x = \pm a$ and between the two parts of the core at $x = x'$) can be written as

$$\vec{G}_1^j\Big|_{x=-a} = \vec{G}_2^j\Big|_{x=-a} \tag{6.6}$$

$$\vec{G}_3^j\Big|_{x=a} = \vec{G}_4^j\Big|_{x=a} \tag{6.7}$$

$$\lim_{x\to x'-} \vec{G}_2^j = \lim_{x\to x'+} \vec{G}_3^j \tag{6.8}$$

$$\vec{D}_r \left.\frac{\partial \vec{G}_1^j}{\partial x}\right|_{x=-a} = \vec{D} \left.\frac{\partial \vec{G}_2^j}{\partial x}\right|_{x=-a} \tag{6.9}$$

$$\vec{D} \left.\frac{\partial \vec{G}_3^j}{\partial x}\right|_{x=-a} = \vec{D}_r \left.\frac{\partial \vec{G}_4^j}{\partial x}\right|_{x=-a} \tag{6.10}$$

$$\lim_{x\to x'+} \frac{\partial G_3^{ij}(x,x',\omega)}{\partial x} - \lim_{x\to x'-} \frac{\partial G_2^{ij}(x,x',\omega)}{\partial x} = \frac{\delta_{ij}}{D^j} \tag{6.11}$$

The boundary conditions can now be recast into a set of matrix equations:

$$\vec{\mathbb{M}}(x',\omega)\vec{A}(x',\omega) = \vec{B} \tag{6.12}$$

where $\vec{B}$ has 12 components, only one of which is non-zero.

Solving the equation analytically is possible, but too cumbersome to do by hand. If done numerically, however, the final solution will only be analytical in x, which meant that it was only a suitable tool when using the adjoint method, where x marked the source. For the direct method, however, x is taken as the detector, and the method is less valuable. However, by using a computer code capable of handling analytical expressions, a solution that was analytical in both x and x' was obtained, meaing that there was no practical difference between using the adjoint and the direct equations.

6.2 Absorption vibration

There are two models for absorption vibration: thin absorbers, modelled as a Dirac distribution, and finite width absorbers, where the noise source is placed at two points in the reactor a short distance apart. Here we will only consider the thin-rod model, and refer to Paper V for the finite width absorber: while their treatment is mathematically different (the finite width absorber case is, in fact, in some ways simpler), the final results are similar.

For a thin absorber, if we assume it to be placed at $x = x_0$ and have a displacement $\varepsilon(t)$, we have a perturbation in the thermal absorption cross section

$$\delta\Sigma_{a2}(x,t) = \gamma(\delta(x - x_0 - \varepsilon(t)) - \delta(x - x_0)). \tag{6.13}$$

The Galanin constant γ describes the strength of the rod; it is not of interest to us here and will be set to unity. In practical applications, localisation of a perturbation is done by taking ratios of detector signals, and the absolute strength of the perturbation will not affect the result.

To get to the frequency domain, we can do a one-term Taylor expansion, and get

$$\delta\Sigma_{a2}(x,\omega) \approx -\gamma\varepsilon(\omega)\delta'(x-x_0). \tag{6.14}$$

The noise from such a perturbation will have both a fast and a thermal component, and then be written as

$$\delta\phi_i(x,\omega) = \gamma\varepsilon(\omega)\left(\phi_2(x_0)\frac{\partial G_{i2}(x,x',\omega)}{\partial x'}\bigg|_{x'=x_0} + G_{i2}(x,x_0,\omega)\,\frac{\partial\phi_2(x')}{\partial x'}\bigg|_{x'=x_0}\right) \tag{6.15}$$

The noise from a central rod (see Fig. 6.1) will of course be symmetrical; the only difference will be in the phase, as the noise can not have any reactivity effect. The shape of the global part of the thermal noise is close to that of the static flux, including reflector peaks. That it is not exactly identical shows that the adiabatic approximation is not applicable for these frequencies.

The fast noise behaves in a similar manner, with a global component which is close to that of the corresponding static flux. However, the local component has a rather peculiar behaviour: as the noise has to be continuous and have opposite phases in the two halves of the reactor, the local component has to be such that the total noise is exactly zero at the perturbation.

If the perturbation is instead placed at some other position (Fig. 6.2), there will also be a third component: a point kinetic term with constant phase. This comes from the rod vibrating at a point where a small displacement to one direction is not equivalent to an equal displacement in the opposite direction.

For an absorber with a finite width d, the results are not very different from those of a thin absorber, except from obvious differences from the width of the perturbation; considering the differences inside the rod is not meaningful as it would be impossible to have a detector there anyway.

6.3 Fuel vibration

Vibration of the fuel rods are more involved than vibration in absorber rods, but not technically more complicated: there are more cross sections to consider, but they are not significantly more difficult to handle. The only difficulty lies in determining the different Galanin constants for the different components, but we shall assume them to be proportional to the corresponding cross sections. Assuming a thin fuel rod, the noise source can then be written as

$$\vec{S}(x,\omega) = -\gamma\varepsilon(\omega)\delta'(x-x_o)\begin{bmatrix} \Sigma_{a1}\phi_1(x) - \left(\nu\Sigma_{f1}\phi_1(x) - \nu\Sigma_{f2}\phi_2(x)\right)\left(1-\frac{i\omega\beta}{i\omega+\lambda}\right) \\ \Sigma_{a2}\phi_2(x) \end{bmatrix}.$$

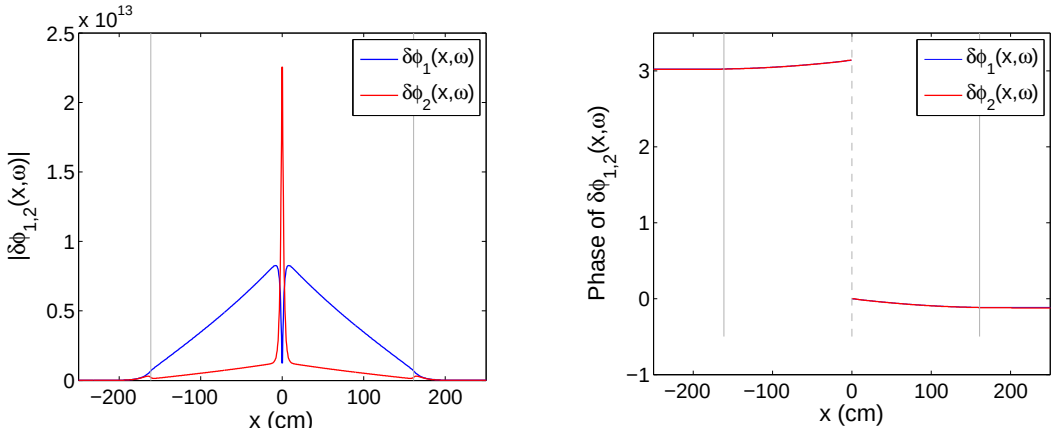

Figure 6.1: Magnitude (left) and phase (right) of the space-dependent noise induced by the vibrations of a thin absorber at $x_0 = 0$, $f = 10$ Hz.

(6.16)

Since we have sources in both the fast and thermal regions, and are detecting both fast and thermal noise, the full Green's function is needed. One can formally divide the noise components depending on their origin (fast or thermal noise source),

$$\delta\phi_i(x,\omega) = \delta\phi_{i1}(x,\omega) + \delta\phi_{i2}(x,\omega) \tag{6.17}$$

Analysing the actual noise from a vibrating central fuel rod (Figs. 6.3 and 6.4), it is seen that while the components from the fast and thermal groups will have similar amplitude, their phase will be opposite. The total noise will thus have a amplitude which is similar in form to these, but the phase will depend on which is dominant. The dominant term can also be shown to be the noise from the same group – i.e. for the thermal noise, the thermal source is more important, and for the fast noise, the fast noise is more important. This further means that the noise from a vibrating fuel rod and that from a vibrating absorber rod will look the same in the thermal region, but will have the opposite phase in the fast region. Thus, by detecting both fast and thermal noise, it is possible to detect which kind of rod is vibrating.

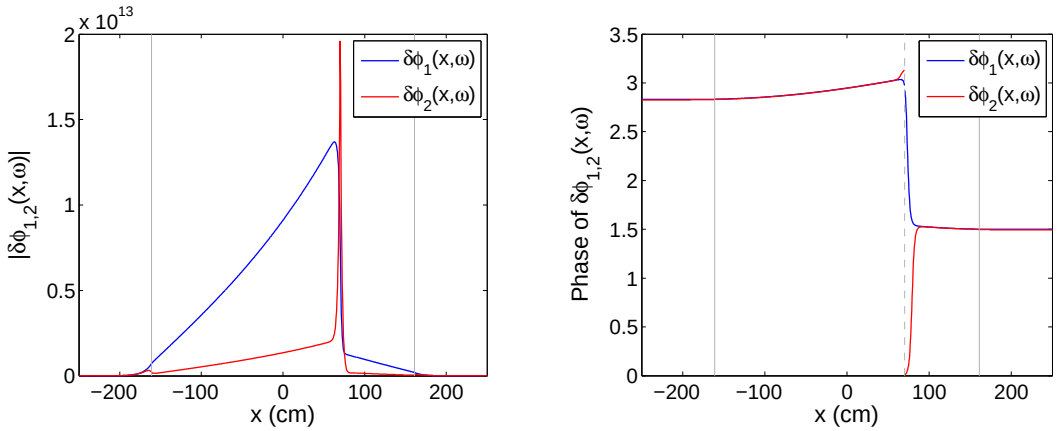

Figure 6.2: Magnitude (left) and phase (right) of the space-dependent noise induced by the vibrations of a thin absorber at $x_0 = 70$ cm, $f = 10$ Hz.

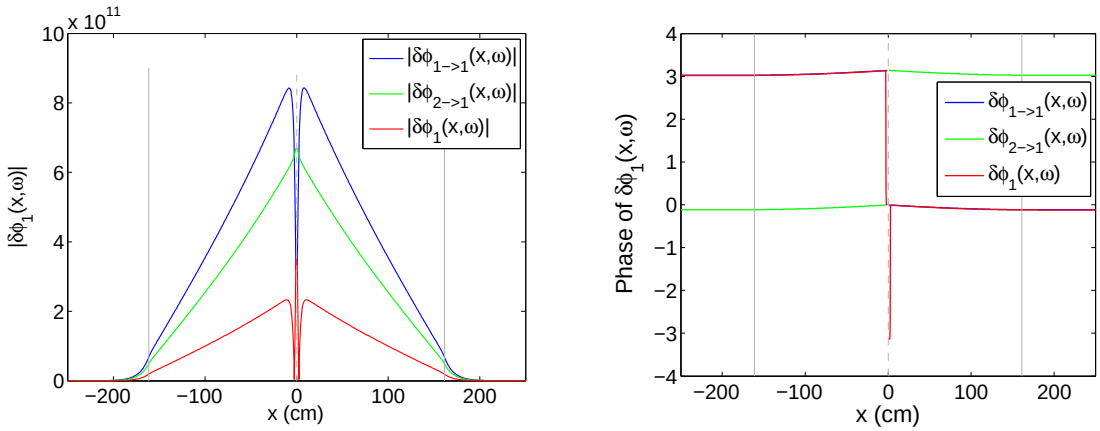

Figure 6.3: Magnitude (left) and phase (right) of the fast noise induced by the vibrations of a thin fuel rod at $x_0 = 0$ cm, $f = 10$ Hz.

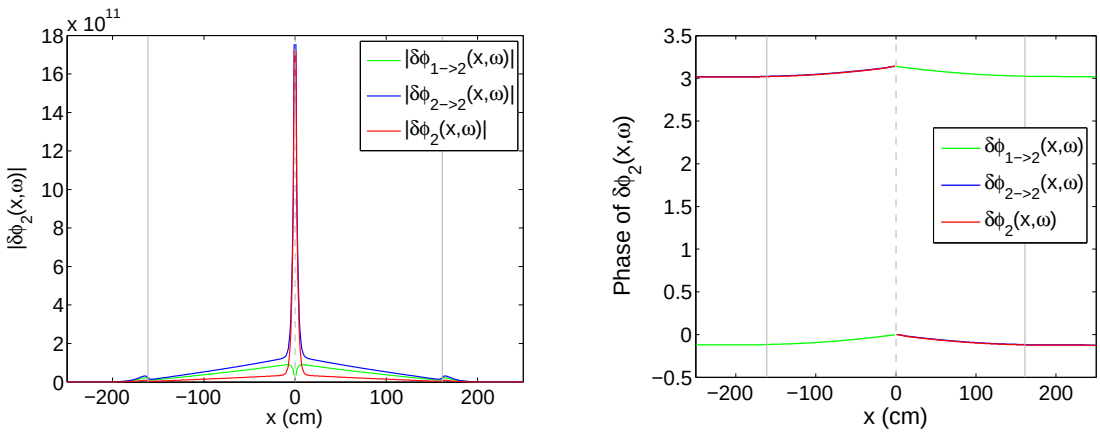

Figure 6.4: Magnitude (left) and phase (right) of the thermal noise induced by the vibrations of a thin fuel rod at $x_0 = 0$ cm, $f = 10$ Hz.

CHAPTER 7

CONCLUDING REMARKS

O most lame and impotent conclusion!
—William Shakespeare, *Othello*

The aim of the research presented here was to identify and investigate any differences between MSRs and traditional reactors, both those that are a result of the moving fuel and those that are a result of different nuclear fuel. The former was mainly done by analysis of a one-group model of a MSR, the latter by analysis of a two-group model. Furthermore, some interesting aspects of the noise that arise as the result of a perturbation propagating through a core that should be valid also for traditional reactors, but have not been seen before, were noted.

The main conclusion that could be drawn is that the induced noise generally has a higher amplitude and that the domain for point-kinetic behaviour is extended up to higher frequencies in a MSR than in a corresponding traditional system, an effect that increases with higher fuel velocities. This can be attributed to two things: the movement of the delayed neutron precursors, which creates an extra coupling between regions in the core, and the lowered effective fraction of delayed neutrons, which makes the prompt neutron chains longer.

Also, even if the validity of the basic point-kinetic theory can be questioned due to asymmetry in the static flux, the results from calculating the noise from a propagating perturbation were still very much like those from traditional reactors, where they can be to a large part explained using point-kinetic theory. On the other hand, point kinetic theory in MSRs are slightly different from that in traditional systems.

The behaviour of thermal thorium-fuelled reactors was also investigated, and it was found that it will differ in some important ways from that of traditional reactors: the use of graphite as a moderator changes the frequency dependence of the induced noise, and the whole reactor shows a much smaller local component of the Green's function. The importance of the local component is also diminished generally in MSRs, due to the more point-kinetic

behaviour. Even so, it plays an important role in the determination of the behaviour of the induced noise from a propagating perturbation.

The use of one- and two-group theory thus did reveal several important properties of MSR, and has also shown possible areas of interest for research for ordinary reactors.

Finally, it has been demonstrated that by using both fast and thermal neutron detectors and observing differences in the phase of an perturbation, it is possible to distinguish between perturbations from absorbers and fuel rods.

ACKNOWLEDGEMENTS

You don't want to make enemies in nuclear engineering.
—Terry Pratchett

I owe thanks to many people, who have been of help directly or indirectly, knowingly or unknowingly, through means I can not list here.

My supervisor, Imre Pázsit, for support and guidance, and for challenging me with new ideas and directions to take the research. Without him, nothing of this would have been possible. Thank you!

Tran Hoai Nam, who has also helped with supervision and has graciously offered to proof-read this thesis. Thank you!

Everyone at the Department of Nuclear Engineering, for friendship and support, discussions that helped me forward, discussions that helped idle away long minutes waiting for results, or just discussions for discussions' sake. This is doubly true for those I have had the fortune to share a room with: Viktor, Larisa, Shuya, Florian, and for the other PhD students: Andreas, Augusto, Britta, Cheuk, Irina, Klara, Petty, Victor. Thank you all!

SKC, for financing this project.

All my friends, without whom these last years would have been very empty. This is especially true for The Thursday Lunch Group (even though it was a while since we had Thursday lunches): Andreas, Magnus, Marcus, Sara and Viktor. Thank you!

Most important of all, my family, for constant love and support. Thank you!

References

I always have a quotation for everything – it saves original thinking.
—Dorothy L. Sayers, *Have his carcase*

[1] H.G. MacPherson. The molten salt reactor adventure. *Nuclear Science and Engineering*, 90:374–380, 1985.

[2] G. H. Marcus. *Nuclear Firsts: Milestones on the Road to Nuclear Power Development*. American Nuclear Society, La Grange Park, Illinois, USA, 2010.

[3] A.M. Weinberg. The proto-history of the molten salt system. *Journal of Accelerator and Plasma Physics*, 2:23–26, 1997.

[4] D. Fishlock. Weinberg's salt reactor. *Nuclear Engineering International*, 52:22–24, 2007.

[5] P.N. Haubenreich. Molten-salt reactors: concepts and technology. *Journal of the British Nuclear Energy Society*, 12(2):145–152, 1973.

[6] G. H. Marcus. *Nuclear Firsts: Milestones on the Road to Nuclear Power Development*. American Nuclear Society, La Grange Park, Illinois, USA, 2010.

[7] J. Krepel. *Dynamics of Molten Salt Reactors*. PhD thesis, Czech Technical University in Prague, 2006.

[8] G. H. Marcus. *Nuclear Firsts: Milestones on the Road to Nuclear Power Development*. American Nuclear Society, La Grange Park, Illinois, USA, 2010.

[9] The Generation IV International Forum. http://www.gen-4.org/.

[10] The US Department of Energy. Generation iv nuclear energy systems. http://www.ne.doe.gov/geniv/neGenIV1.html.

[11] C.D. Bowman. Once-through thermal-spectrum accelerator-driven light water reactor waste destruction without reprocessing. *Nuclear Technology*, 132:66–93, 2000.

[12] P.N. Alekseev, V.V. Ignatiev, S.A. Konakov, L.I. Menshikov, N.N. Ponomarev-Stepnoi, V.N. Prusakov, V.A. Stukalov, and S.A. Subbotine. Harmonization of fuel cycles for nuclear energy system with the use of molten salt technology. *Nuclear Engineering and Design*, 173:151–158, 1997.

[13] J. Vergnes and D. Lecarpentier. The amster concept (actinides molten salt transmuter). *Nuclear Engineering and Design*, 216:43–67, 2002.

[14] S. Dulla, P. Ravetto, and M.M. Rostagno. Neutron kinetics of fluid-fuel systems by the quasi-static method. *Annals of Nuclear Energy*, 31(15):1709–1733, 2004.

[15] J. Krepel, U. Rohde, U. Grundmann, and F-P. Weiss. Dynamics of molten salt reactors. *Nuclear Technology*, 164:34–44, 2007.

[16] R.W. Moir. Cost of electricity from molten salt reactors. *Nuclear Technology*, 138:93–95, 2002.

[17] S. David, E. Huffer, and H. Nifenecker. Revisting the thorium-uranium fuel cycle. *Euro Physics News*, 38(2):34–27, 2007.

[18] T. Kamei and Hakami S. Evaluation of implementation of thorium fuel cycle with lwr and msr. *Progress in Nuclear Energy*, 53:820–824, 2011.

[19] U. Gat and J.R. Engel. Non-proliferation attributes of molten salt reactors. *Nuclear Engineering and Design*, 201:327–334, 2000.

[20] L. Mathieu, P.N. Alekseev, V.V. Ignatiev, S.A.Konakov, L.I. Menshikov, N.N.Ponomarev-Stepnoi, V.N.Prusakov, V.A. Stukalov, S.A. Subbotine, D. Heuer, R. Brissot, C. Garzenne, C. Le Brun, D. Lecarpentier, E. Liatard, J.-M. Loiseaux, O. Méplan, E. Merle-Lucotte, A. Nuttin, E. Walle, and J. Wilson. The thorium molten salt reactor: Moving on from the msbr. *Progress in Nuclear Energy*, 48:664–679, 2006.

[21] R. V. Meghreblian and D.K. Holmes. *Reactor Analysis*. McGraw Hill, New York, 1960.

[22] S. Dulla. *Models and methods in the neutronics of fuel fluid reactors*. PhD thesis, Politecnico di Turino, 2005.